Journal of Organometallic Chemistry 696 (2011) 3623–3636

Contents lists available at SciVerse ScienceDirect

Journal of Organometallic Chemistry

journal homepage: www.elsevier.com/locate/jorganchem

Preparation, properties, and reactivity of carbonylrhodium(I) complexes of di(2-pyrazolylaryl)amido-pincer ligands

Sarath Wanniarachchi, Brendan J. Liddle, Sergey V. Lindeman, James R. Gardinier*

Department of Chemistry, Marquette University, Milwaukee, WI 53201-1881, United States

ARTICLE INFO

Article history:
Received 2 August 2011
Received in revised form
14 August 2011
Accepted 16 August 2011

Keywords:
NNN pincer ligands
Copper-catalyzed amination
Carbonylrhodium(I)
IR spectroscopy
Oxidative addition

ABSTRACT

A series of six carbonylrhodium(I) complexes of three new and three previously reported di(2-3R-pyrazolyl)-*p*-Z/X-aryl)amido pincer ligands, (^{R}ZX)Rh(CO), (R is the substituent at the 3-pyrazolyl position proximal to the metal; Z and X are the aryl substituents *para*- to the arylamido nitrogen) were prepared. The metal complexes were studied to assess how their properties and reactivities can be tuned by varying the groups along the ligand periphery and how they compared to other known carbonylrhodium(I) pincer derivatives. This study was facilitated by the discovery of a new CuI-catalyzed coupling reaction between 2-(pyrazolyl)-4-X-anilines (X = Me or CF_3) and 2-bromoaryl-1*H*-pyrazoles that allow the fabrication of pincer ligands with two different aryl arms. The NNN-pincer scaffolds provide an electron-rich environment for the carbonylrhodium(I) fragment as indicated by carbonyl stretching frequencies that occur in the range of 1948–1968 cm^{-1}. As such, the oxidative addition (OA) reactions with iodomethane proceed instantaneously to form *trans*-(NNN-pincer)Rh(Me)(CO)(I) in room temperature acetone solution. The OA reactions with iodoethane proceeded at a convenient rate in acetone near 45 °C which allowed detailed kinetic studies. The relative order of reactivity was found to be (CF_3CF_3)Rh(CO) < (^{iPr}MeMe)Rh(CO) < (^{Me}MeMe)Rh(CO) ~ (CF_3Me)Rh(CO) < (MeH)Rh(CO) < (MeMe)Rh(CO) with the second order rate constant of the most reactive in the series, $k_2 = 8 \times 10^{-3}$ M^{-1} s^{-1}, being about three orders of magnitude greater than those reported for $[Rh(CO)_2I_2]^-$ or CpRh(CO)(PPh_3). After oxidative addition, the resultant rhodium(III) complexes were found to be unstable. Although a few *trans*-(^{R}MeMe)Rh(E = Me, Et, or I)(CO)(I) could be isolated in pure form, all were found to slowly decompose in solution to give different products depending on the 3R-pyrazolyl substituents. Those with unsubstituted pyrazolyls (R = H) decompose with CO dissociation to give insoluble dimeric [(^{R}MeMe)Rh(E)(μ-I)]$_2$ while those with 3-alkylpyrazolyls (R = Me, ^{i}Pr) decompose to give soluble, but unidentified products.

© 2011 Elsevier B.V. All rights reserved.

1. Introduction

Since the seminal report by Moulton and Shaw of rhodium(I) and other metal complexes of uni-negative, meridonially-coordinating 'pincer' ligands with PCP-donors in 1976 [1], the chemistry of rhodium(I) pincer complexes has remained affixed among the more popular contemporary investigations given the historical importance of low-valent rhodium complexes in the Monsanto process for the production of acetic acid from methanol. Part of the appeal of pincer complexes arises from their relatively high stability and unusual chemistry that can be promoted by judicious ligand designs [2]. Early reports by van Koten's group concerning metal complexes of NCN-pincer variants demonstrated that exciting new chemistry was attainable by varying donor groups [3]. In particular, van Koten's observations regarding rhodium NCN-pincer complexes [4] presaged numerous contemporary discoveries that other rhodium pincer complexes are competent for the activation of normally robust C–X (X = halide), C–H, N–C, N–H, and H–H bonds [5]. Notable rhodium pincer complexes that show unusual chemistry typically have an anchoring amido nitrogen with two flanking phosphorus donors such as in (PNP)Rh derivatives by the groups of Liang [6], Ozerov [7], Mayer and Kaska [8], Milstein [9], or Caulton [10]. Other fascinating chemistry is found by replacing one or more of the donor groups with different atoms, as in (PCP)Rh derivatives [11,12], the (PSiP)Rh derivatives of Turculet [13], or the various (SPS)Rh derivatives of the Cauzzi [14] and LeFloch groups [15]. More exotic donors are found in the (NBN)Rh derivatives of Nakamura [16], the (CNC)Rh derivative with flanked olefin donors described by Grützmacher [17] or that with *N*-heterocyclic carbene donors as in Kunz's 1,8-bis(imidazolin-2-yliden-1-yl)carbazolide (bimca) derivatives [18].

* Corresponding author.
E-mail address: james.gardinier@marquette.edu (J.R. Gardinier).

0022-328X/$ – see front matter © 2011 Elsevier B.V. All rights reserved.
doi:10.1016/j.jorganchem.2011.08.013

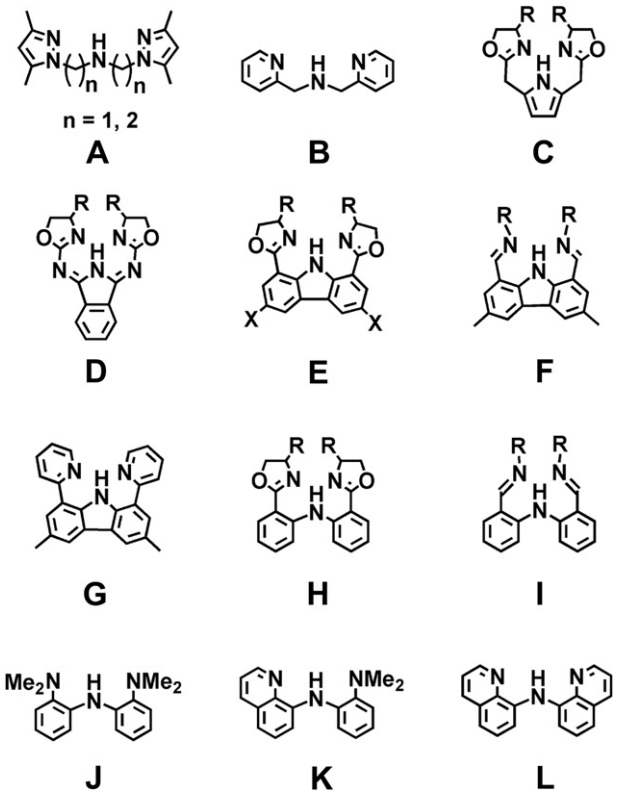

Chart 1. Selected examples of NNN-pincer ligands in the literature.

There has been growing interest in the development of late transition metal complexes of pincer ligands that possess an NNN donor set (Chart 1) since nitrogen donors tend to be more resistant to oxidative degradation versus phosphine donors and because it is thought that the dichotomy between hard Lewis donors and soft rhodium(I) center could lead to enhanced or unexpected reaction chemistry relative to derivatives with soft Lewis donors. Although many examples of metal complexes of NNN pincer ligands are known [19–30], studies of their low-valent rhodium chemistry are relatively limited. For instance, of the twelve representative classes of ligand **A**–**L** in Chart 1, low-valent rhodium chemistry has only been described for five (**A** [19], **B** [20], **C** [21], **D** [22], and **F** [24]). Of these, the oxidative addition reactions of (**C**)Rh(CO) and (**F**)Rh(CO) have been addressed where it was found that the electron-rich character of the NNN-ligand substantially increased the rate of iodomethane oxidative addition relative to the traditional Monsanto catalyst $[Rh(CO)_2(I)_2]^-$. Unfortunately, the effect of different R groups on the rates of oxidative addition of iodomethane or of other alkyl halides or the implementation of complexes such as (**F**)Rh(CO) in catalytic reactions have not yet been reported.

We recently reported a set of three new di(2-(3R-pyrazolyl-1-yl)-4-tolyl)amine NNN-pincer ligands, H(^{R}MeMe) (R = H, Me, ^{i}Pr), whose notation is defined in Fig. 1 [31]. In those reports we documented some unusual ligand-centered chemistry of *fac*-tricarbonylrhenium(I) complexes that arose from the unconventional coordination geometry of the pincer ligand enforced by both the *fac*-Re(CO)$_3$ moiety and the steric bulk of the R groups at the 3-position of the pyrazolyl (Fig. 1). We were interested to begin investigation of rhodium(I) derivatives of these new pincer ligands because metal-centered chemistry was anticipated for potential square planar complexes. Specifically, we wanted to get a sense of how the reactivity of the new complexes toward iodoalkanes would compare to other rhodium(I) pincers and of the extent that the reactivity could be attenuated by making changes to the groups decorating the new ligand scaffold. In this report, we describe an important advance in ligand syntheses that provides a simple, convergent means to prepare (2-pyrazolyl)aryl-containing ligands that have different pincer 'arms'. Also, we provide a full account of the preparation and properties of six carbonylrhodium(I) complexes; (MeMe)Rh(CO), **1**, (^{Me}MeMe)Rh(CO), **2**, (^{iPr}MeMe)Rh(CO), **3**, (MeH)Rh(CO), **4**, (MeCF$_3$)Rh(CO), **5**, and (CF$_3$CF$_3$)Rh(CO), **6**. The oxidative addition reactions involving **1**–**6** and iodoalkanes and, in one case iodine, were probed to delineate the effects of ligand sterics and electronics on the kinetics and thermodynamic outcomes of OA reactions. These results provide a benchmark for our future work with related pincer variants.

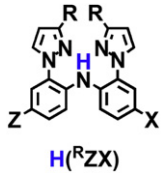

Fig. 1. General representation and notation of the NNN-pincer ligands used in this work. When R = H, the superscript R is omitted.

2. Experimental

2.1. Materials

Pyrazole, CuI, *N*,*N*′-dimethylethylenediamine (DMED), anhydrous M_2CO_3 powders (M = K, Cs), 1-bromo-2-fluoro-4-trifluoromethylbenzene, 1-bromo-2-fluorobenzene, NaH, and Li(*n*-Bu) (1.6 M in hexane) were purchased from commercial sources and used without further purification while $[(CO)_2Rh(\mu\text{-}Cl)]_2$ [32], $Rh(CO)_2(acac)$ [33], H(MeMe) [31b], H(^{Me}MeMe) [31a], and H(^{iPr}MeMe) [31a], H(pzAn^{X}) (pzAn^{X} = 2-(pyrazolyl)-*p*-X-aniline; X = CF_3, CH_3) [34] were prepared by literature methods. Commercial methyl- and ethyl iodide were dried over $CaCl_2$ and distilled under vacuum before use. Solvents used in the preparations were dried by conventional methods and were distilled under nitrogen prior to use.

2.2. Physical measurements

Midwest MicroLab, LLC, Indianapolis, Indiana 45250, performed all elemental analyses. ^{1}H, ^{13}C and ^{19}F NMR spectra were recorded on a Varian 400 MHz spectrometer. Chemical shifts were referenced to solvent resonances at δ_H 7.26 and δ_C 77.23 for $CDCl_3$, δ_H 5.32 and δ_C 53.84 for CD_2Cl_2, δ_H 2.05 and δ_C 29.92 for acetone-d_6. Infrared spectra were recorded on samples as either KBr pellets or as acetone solutions with cells having KBr windows using a Nicolet Magna-IR 560 spectrometer. Melting point determinations were made on samples contained in glass capillaries using an Electrothermal 9100 apparatus and are uncorrected. Mass spectrometric measurements recorded in ESI(+) mode were obtained on a Micromass Q-TOF spectrometer whereas those performed by using direct-probe analyses were made on a VG 70S instrument. For the ESI(+) experiments, formic acid (approximately 0.1% v/v) was added to the mobile phase (CH_3CN).

2.3. Synthesis of 2-bromoarylpyrazole precursors

2.3.1. Synthesis of 1-(2-bromophenyl)-1H-pyrazole, BrPhpz

A solution of 3.53 g (0.0518 mol) pyrazole in 20 mL of dry DMF was slowly transferred to a suspension of 1.24 g (0.0518 mol) NaH in 30 mL of dry DMF to control the rate of hydrogen evolution. After complete addition the solution was stirred for 15 min and then 7.56 g

(0.0432 mol) of 1-bromo-2-fluorobenzene in 10 mL of dry DMF was added by cannula transfer and the mixture was heated at reflux for 30 min. After cooling to room temperature 200 mL of water was added and the mixture was extracted with three 50 mL portions of CH_2Cl_2. The combined organic layers were then washed with five 50 mL portions water and the organic phase was dried over $MgSO_4$ and was filtered. The solvent was removed by vacuum distillation to leave an oily residue. The oily residue was subjected to column chromatography on silica gel where the desired product ($R_f = 0.6$ on SiO_2 plate) was isolated as a colorless oil (8.34 g, 86%) using 6:1 hexane:ethyl acetate as an eluent. ^{1}H NMR ($CDCl_3$): δ_H 7.82 (dd, $J = 2.4$, 0.6 Hz, 1H), 7.76 (dd, $J = 1.8$, 0.4 Hz, 1H), 7.71 (m, 1H), 7.52 (m, 1H), 7.42 (m, 1H), 7.28 (m, 1H), 6.47 (dd, $J = 2.4$, 1.8 Hz, 1H) ppm. ^{13}C NMR ($CDCl_3$): δ_C 141.0, 140.0, 133.9, 131.4, 129.7, 128.5, 128.4, 118.7, 106.6 ppm.

2.3.2. Synthesis of 2-bromo-5-trifluoromethylphenyl-1H-pyrazole, Br–CF_3Phpz

Similar to above, the reaction between 4.20 g (0.0617 mol) pyrazole, 1.63 g (0.0679 mol) NaH and 15.0 g (0.0618 mol) of 1-bromo-2-fluoro-4-trifluoromethylbenzene gave an oily residue after work-up that was subjected to column chromatography on silica gel. The desired product ($R_f = 0.75$ on SiO_2 plate) was separated from a more polar, but unidentified, impurity ($R_f = 0.5$ on SiO_2 plate) using 6:1 hexane:ethyl acetate as an eluent. Removal of solvents under vacuum afforded 10.16 g (57% based on pyrazole) of Br–CF_3Phpz as a colorless oil. ^{1}H NMR: ($CDCl_3$): δ_H 7.90 (d, $J = 2$ Hz, 1H, H_5pz), 7.83(m, 2H, Ar), 7.78 (d, $J = 2$ Hz, 1H, H_3pz), 7.52 (part of *AB*, $J_{app} = 8$, 2 Hz, 1H, Ar), 6.51 (t, $J = 2$ Hz, 1H, H_4pz) ppm. ^{13}C NMR ($CDCl_3$): δ_C 141.7, 140.4, 134.8, 131.4, 131.1 (q, $^2J_{C-F} = 33$ Hz), 126.1 (q, $^3J_{C-F} = 3$ Hz), 125.4 (q, $^3J_{C-F} = 3$ Hz), 123.4 (q, $^1J_{C-F} = 272$ Hz), 122.1 (q, $^4J_{C-F} = 2$ Hz), 107.4 (C_4pz) ppm. ^{19}F NMR ($CDCl_3$): δ_F −62.8 ppm.

2.4. Synthesis of new pincer ligands

2.4.1. Synthesis of N-(4-methyl-2-(1H-pyrazol-1-yl)phenyl)-2-(1H-pyrazol-1-yl)benzenamine, H(MeH)

A Schlenk flask was charged with 2.238 g (0.0129 mol) H(pzAn^{Me}), 3.455 g (0.0155 mol, 1.2 eq) BrPhpz, 5.047 g (0.0155 mol, 1.2 eq) Cs_2CO_3 and was deoxygenated by three evacuation and nitrogen back-fill cycles. Then 30 mL of dioxane and 0.492 g (2.581 mmol, 20 mol %) CuI were added under nitrogen blanket. The reaction mixture was heated at reflux for 15 h under nitrogen. After cooling to room temperature, dioxane was removed by vacuum distillation. The solid product mixture was extracted with four 20 mL portions of Et_2O and then Et_2O was removed by vacuum distillation to afford a residue that was further purified by column chromatography on silica gel. After elution with 6:1 hexane:ethyl acetate ($R_f = 0.4$) and removal of solvents the desired product was obtained as a white solid. Yield: 2.957 g, 73%. M.p.: 63–65 °C Anal. Calcd. for $C_{19}H_{17}N_5$: C, 72.37; H, 5.43; N, 22.21. Found: C, 72.21; H, 5.64; N, 22.11. ^{1}H NMR (acetone-d_6): δ_H 9.11 (s), 7.92 (m, 2 H), 7.76 (dd, $J = 2.0$, 1.7 Hz, 1H), 7.72 (d, $J = 2$ Hz, 1H), 7.37 (m, 3 H), 7.26 (m, 1 H), 7.33 (m, 1 H), 7.12 (dd, $J = 8.3$, 1.3 Hz, 1 H), 6.94 (m, 1 H), 6.49 (t, $J = 2.1$ Hz, 1 H), 6.46 (t, $J = 2.1$ Hz, 1 H), 2.32(s, 3 H) ppm. ^{13}C NMR (acetone-d_6): δ_c 141.13, 141.08, 140.6, 138.5, 134.7, 131.94, 131.85, 130.9, 130.7, 129.4, 129.0, 126.4, 125.9, 121.0, 120.5, 118.3, 107.32, 107.27, 20.5 ppm.

2.4.2. Synthesis of N-(4-(trifluoromethyl)-2-(1H-pyrazol-1-yl) phenyl)-4-methyl-2-(1H-pyrazol-1-yl)benzenamine, H(MeCF$_3$)

A Schlenk flask was charged with 0.784 g (4.53 mmol) H(pzAn^{Me}), 1.581 g (5.43 mmol, 1.2 eq) Br-CF_3Phpz, 1.770 g (5.43 mmol, 1.2 eq) Cs_2CO_3 and was deoxygenated by three evacuation and nitrogen back-fill cycles. Then, 15 mL of dry dioxane and 0.173 g (0.905 mmol, 20 mol %) CuI were added under a nitrogen blanket. The reaction mixture was heated at reflux for 15 h under nitrogen. After cooling to room temperature, dioxane is removed by vacuum distillation. The solid product mixture was extracted with four 20 mL portions of Et_2O (until filtrate was nearly colorless) and then Et_2O was removed by vacuum distillation to afford a residue that was further purified by column chromatography on silica gel. After elution with 6:1 hexane:ethyl acetate ($R_f = 0.38$) and removal of solvents by vacuum distillation, the desired product was obtained as a beige solid. Recrystallization by cooling hot supersaturated hexane solutions to room temperature over the course of several hours afforded 1.432 g (83%) of H(MeCF$_3$) as colorless needles. M.p.: 79–82 °C. Anal. Calcd. for $C_{20}H_{16}F_3N_5$: C, 62.66; H, 4.21; N, 18.27. Found: C, 62.69; H, 4.29; N, 18.41. ^{1}H NMR ($CDCl_3$): δ_H 9.03 (br s, 1H, NH), 7.78 (dd, 1H, $J = 2$, 1 Hz, H_5pz–ArCF_3), 7.76 (dd, 1H, $J = 2$, 1 Hz, H_3pz–ArCF_3), 7.70 (dd, $J = 2$, 1 Hz, 1H, H_5pz–tolyl), 7.67 (dd, 1H, $J = 2$, 1 Hz, H_3pz–tolyl), 7.50 (d, $J = 2$ Hz, 1H, H–ArCF_3), 7.40 (part of *AB*, $J_{app} = 8$ Hz, 1H, ArCF_3), 7.38 (part of *AB*, $J_{app} = 8$, 1 Hz, 1H, ArCF_3), 7.31 (part of *AB*, $J_{app} = 8$ Hz, 1H, tolyl), 7.25 (d, $J = 1$ Hz, 1H, tolyl), 7.13 (part of *AB*, $J_{app} = 8$, 2 Hz, 1H, ArCF_3), 6.51 (t, $J = 2$ Hz, 1H, H_4pz–ArCF_3), 6.40 (t, $J = 2$ Hz, 1H, H_4pz–tolyl), 2.36 (s, 3H, CH_3) ppm. ^{13}C NMR ($CDCl_3$): δ_C 141.4, 141.2, 140.7, 133.7, 132.4, 131.9, 130.2, 129.8, 128.9, 127.9, 125.9, 125.5 (q, $^3J_{C-F} = 4$ Hz), 124.2 (q, $^1J_{C-F} = 271$ Hz, CF_3), 122.3 (q, $^3J_{C-F} = 4$ Hz), 122.2, 120.9 (q, $^2J_{C-F} = 33$ Hz), 115.4, 107.3 (C_4pz–ArCF_3), 106.9 (C_4pz–tolyl), 20.8 ppm ^{19}F NMR ($CDCl_3$): δ_F −61.4 ppm.

2.4.3. Synthesis of bis(4-(trifluoromethyl)-2-(1H-pyrazol-1-yl) phenyl)amine, H(CF_3CF_3)

Similar to above, a deoxygenated mixture of 0.652 g (2.87 mmol) H(pzAn^{CF3}), 1.002 g (3.44 mmol, 1.2 eq) Br–CF_3Phpz, 1.122 g (3.44 mmol, 1.2 eq) Cs_2CO_3, and 0.110 g (0.578 mmol, 20 mol %) CuI in 15 mL of dioxane was heated at reflux for 15 h under nitrogen. After cooling to room temperature, dioxane was removed by vacuum distillation. The solid product mixture was extracted with four 20 mL portions of Et_2O (or until filtrate was nearly colorless) and then Et_2O was removed by vacuum distillation to afford a residue that was further purified by column chromatography on silica gel. Elution of the column with 6:1 hexane:ethyl acetate ($R_f = 0.47$) and removal of solvents by vacuum distillation gave the desired product as a tan solid. After recrystallization by cooling hot supersaturated hexane solutions to room temperature over the course of several hours afforded 1.125 g (90%) of H(CF_3CF_3) as white needles. M.p.: 89–91 °C. Anal. Calcd. for $C_{20}H_{13}F_6N_5$: C, 54.94; H, 3.10; N, 16.01. Found: C, 54.94; H, 3.10; N, 15.96. ^{1}H NMR ($CDCl_3$): δ_H 9.76 (br s, 1H, NH), 7.77 (d, $J = 3$ Hz, 2H, H_5pz), 7.76 (d, $J = 2$ Hz, 2H, H_3pz), 7.60 (s, 2H, Ar), 7.58 (part of *AB*, $J_{app} = 8$ Hz, 2H, Ar), 7.50 (part of *AB*, $J_{app} = 8$ Hz, 2H, Ar), 6.51 (dd, $J = 3$, 2 Hz, 2H, H_4pz) ppm. ^{13}C NMR ($CDCl_3$): δ_C 141.4, 139.0, 138.9, 130.1, 125.4 (q, $^3J_{C-F} = 4$ Hz), 123.8 (q, $^1J_{C-F} = 271$ Hz, CF_3), 123.6 (q, $^2J_{C-F} = 34$ Hz), 122.6 (q, $^3J_{C-F} = 4$ Hz), 118.5, 107.6 (C_4pz) ppm. ^{19}F NMR ($CDCl_3$): δ_F −61.9 ppm.

2.5. Synthesis of carbonylhodium(I) complexes

2.5.1. Synthesis of (MeMe)Rh(CO), **1**

2.5.1.1. Method A. A mixture of 0.2079 g (0.632 mmol) H(MeMe) and 0.1629 g (0.632 mmol) $Rh(CO)_2$(acac) in 15 mL of dry, deoxygenated acetone was heated at reflux for 30 h under nitrogen. After cooling to room temperature, the volatile components were removed under vacuum to give 0.2398 g (83%) of pure **1** as a yellow, crystalline solid.

2.5.1.2. Method B. A 2.6 mmol portion of Li(*n*-Bu) (1.6 mL of a 1.6 M solution in hexane) was added to a solution of 0.847 g (2.57 mmol) of H(MeMe) in 15 mL THF at −78 °C. The resultant yellow solution

was stirred at −78 °C for 30 min and a solution of 0.500 g (1.29 mmol) $[(CO)_2Rh(\mu\text{-}Cl)]_2$ in 15 mL THF was subsequently added via cannula transfer. After the resulting red-brown solution had been stirred at −78 °C for an additional 30 min, the cold bath was removed and stirring was continued an additional 14 h. Solvent was then removed under vacuum to leave a brown solid. The brown solid was washed with hot pentane to remove any H(MeMe) and the filtrate was reserved (vide infra). The solid was then extracted with dry toluene and the solvent was removed under vacuum to give 0.373 g (32%) of **1** as a yellow powder. The original pentane extract contained an additional fraction 0.140 g (12%) of **1** which slowly crystallized on standing. The combined yield of **1** from the toluene and pentane extracts was 0.513 g (44%). M.p.: 280–283 °C (dec.) Anal. Calcd. for $C_{21}H_{18}N_5ORh$: C, 54.91; H, 3.96; N, 15.25. Found: C, 55.26; H, 4.02; N, 15.03. ^{1}H NMR (acetone-d_6): δ_H 8.45 (d, $J = 2$ Hz, 2H, H_3pz), 7.83 (d, $J = 2$ Hz, 2H, H_5pz), 7.30 (s, 2H, Ar), 6.95 (part of *AB*, 2H, Ar), 6.88 (part of *AB*, 2H, Ar), 6.67 (t, $J = 2$, 2H, H_4pz), 2.26 (s, 6H, $ArCH_3$). ^{13}C NMR (acetone-d_5): δ_C 193.1 (d, $^1J_{Rh-C} = 72$ Hz, CO), 146.6 (d, $^3J_{Rh-C} = 3$ Hz), 143.5, 130.5, 130.1 (d, $^3J_{Rh-C} = 1$Hz), 129.7, 127.5, 123.6, 123.4, 108.7 (d, $^3J_{Rh-C} = 2$Hz, C_4pz), 20.4. IR (ν_{CO}, cm^{-1}): 1952 (KBr pellet); 1955 (acetone). LRMS (Direct Probe, *m*/*z*) (int.) [assign.]: 459 (52) $[LRh(CO)]^{\bullet+}$, 431 (100) $[LRh]^{\bullet+}$, 329 (40) $[HL]^+$. X-ray quality crystals were obtained by layering a benzene solution with pentane and allowing solvents to slowly diffuse over 12 h. Alternatively, slow evaporation of saturated pentane solution of **1** was a successful approach.

2.5.2. Synthesis of (^{Me}MeMe)Rh(CO), **2**

2.5.2.1. Method A. Heating mixture of 0.179 g (0.499 mmol) H(^{Me}MeMe) and 0.129 g (0.499 mmol) $Rh(CO)_2$(acac) in 15 mL acetone for 30 h, then removing volatiles under vacuum gave 0.243 g (87%) of pure **2** as a yellow crystalline solid.

2.5.2.2. Method B. In a manner similar to that described for **1**, 0.619 g (1.70 mmol) H(^{Me}MeMe), 1.76 mmol Li(*n*-Bu) (1.10 mL, 1.6 M in hexane) and 0.337 g (1.73 mmol) $[(CO)_2Rh(\mu\text{-}Cl)]_2$ in 30 mL THF gave 0.171 g (20%) of **2** as a yellow powder after work-up. M.p.: 260–262 °C (dec.) Anal. Calcd. (obsd.) for $C_{23}H_{22}N_5ORh$: C, 56.68; H, 4.55; N, 14.37. Found: C, 56.52; H, 4.56; N, 14.15. ^{1}H NMR (acetone-d_6): δ_H 8.23 (d, $J = 2$ Hz, 2H, H_5pz), 7.29 (s, 2H, Ar), 6.82 (both parts of *AB*, 4H, Ar), 6.53 (d, $J = 2$, 2H, H_4pz), 2.48 (s, 6H, $pzCH_3$), 2.26 (s, 6H, $ArCH_3$) ppm. ^{13}C NMR (acetone-d_5): δ_C 193.6 (d, $^1J_{Rh-C} = 70$ Hz, Rh–CO), 153.5 (d, $^2J_{Rh-C} = 2$ Hz), 142.7, 132.2, 131.1 (d, $^3J_{Rh-C} = 1$ Hz), 129.4, 127.0, 122.8, 122.3, 109.8 (d, $^3J_{Rh-C} = 2$ Hz, C_4pz), 20.5, 17.2 ppm. IR (ν_{CO}, cm^{-1}): 1952 (KBr pellet); 1951 (acetone). LRMS (Direct Probe, *m*/*z*) (int.) [assign.]: 487 (28) $[LRh(CO)]^{\bullet+}$, 459 (100) $[LRh]^{\bullet+}$, 444 (16) $[LRh-CH_3]^{\bullet+}$, 357 (8) $[HL]^+$.

2.5.3. Synthesis of (^{iPr}MeMe)Rh(CO), **3**

Under nitrogen, a 0.75 mmol sample of Li(*n*-Bu) (0.47 mL of 1.6 M solution in hexane) was added dropwise by syringe to a solution of 0.31 g (0.75 mmol) H(^{iPr}MeMe) in 15 mL toluene at −78 °C. After stirring at −78 °C for 10 min, a solution of 0.146 g (0.375 mmol) $[(CO)_2Rh(\mu\text{-}Cl)]_2$ in 15 mL toluene was added dropwise via cannula transfer. After complete addition, the mixture was stirred at −78 °C for 4 h then the cold bath was removed. After the mixture was stirred an additional 15 h, the volatile components were removed by vacuum distillation to leave a brown solid. The solid was extracted using five 20 mL portions of pentane and filtering from the brown insoluble solid (until the extracts were colorless). The desired yellow product slowly crystallized from the pentane extracts on standing. Several crops of pure crystalline **3** were collected after four cycles of decanting the mother liquor, concentrating the solution by rotary evaporation to half volume, and crystallization. The crystals were dried under vacuum to give a total of 0.152 g (37% based on H(^{iPr}MeMe)). M.p.: 227–230 °C (dec.) Anal. Calcd. for $C_{27}H_{30}N_5ORh$: C, 59.67; H, 5.56; N, 12.89.Found: C, 59.80; H, 5.71; N, 12.85. ^{1}H NMR (acetone-d_6): δ_H 8.28 (d, $J = 3$ Hz, 2H, H_5pz), 7.29 (s, 2H, Ar), 6.83 (part of *AB*, 2H, Ar), 6.79 (part of *AB*, 2H, Ar), 6.63 (d, $J = 3$ Hz, 2H, H_4pz), 3.56 (sept, $J = 7$ Hz, 2H, $CHMe_2$), 2.25 (s, 6H, $ArCH_3$), 1.32 (d, $J = 7$ Hz, 6H, $^iPrCH_3$). 1.30 (d, $J = 7$ Hz, 6H, $^iPrCH_3$) ppm. ^{13}C NMR (acetone-d_5): δ_C 193.5 (d, $^1J_{Rh-C} = 70$ Hz, Rh–CO), 163.8 (d, $^2J_{Rh-C} = 2$ Hz), 142.7, 132.8, 131.2, 129.4, 126.9, 122.8, 121.8, 106.1 (d, $^3J_{Rh-C} = 2$ Hz, C_4pz), 23.8, 23.3, 20.5 ppm. IR (ν_{CO}, cm^{-1}): 1948 (KBr pellet); 1948 (acetone). LRMS (Direct Probe, *m*/*z*) (int.) [assign.]: 543 (31) $[LRh(CO)]^{\bullet+}$, 515 (100) $[LRh]^{\bullet+}$, 413 (12) $[HL]^+$.

2.5.3.1. Attempted preparations by method A. Reactions between H(^{iPr}MeMe) and $Rh(CO)_2$(acac) were only 45–50% complete after 3 days according NMR-scale reactions. Moreover, the similar solubilities of the rhodium-containing reagent and product hindered separation and only allowed isolation of trace quantities of pure **3** by this route even from half-gram scales of reagents.

2.5.4. Synthesis of (MeH)Rh(CO), **4**

Heating mixture of 0.236 g (0.749 mmol) H(MeH) and 0.193 g (0.749 mmol) $Rh(CO)_2$(acac) in 20 mL acetone for 60 h, then removing volatiles under vacuum gave 0.282 g (84%) of pure (MeH)Rh(CO) as a yellow crystalline solid. M.p.: 220–225 °C (dec.). Anal. Calcd. for $C_{20}H_{16}N_5ORh$: C, 53.95; H, 3.62; N, 15.73. Found: C, 54.05; H, 3.71; N, 15.63. ^{1}H NMR (acetone-d_6): δ_H 8.47 (d, $J = 2.8$ Hz, 1 H), 8.45 (d, $J = 2.8$ Hz, 1H), 7.84 (m, 2 H), 7.44 (m, 2 H), 7.32 (m, 1 H), 7.03 (m, 2 H), 6.97 (m, 1 H), 6.91 (m, 1 H), 6.76–6.67 (m, 3 H), 2.27 (s, 3 H). ^{13}C NMR (acetone-d_6): δ_C 192.56 (d, $J_{Rh-CO} = 71$ Hz), 146.72 (d, $J = 2.7$ Hz), 146.60 (d, $J = 2.8$ Hz), 146.21, 143.15, 130.62, 130.61, 130.44 (d, $J = 1.2$ Hz), 130.41 (d, $J = 1.2$ Hz), 129.82, 128,84, 128.18, 123.76, 123.72, 123.53, 123.15, 117.88, 108.86 (d, $J = 2.2$ Hz), 108.81 (d, $J = 2.2$ Hz), 20.43. IR (ν_{CO}, cm^{-1}): 1954 (KBr pellet), 1956 (acetone).

2.5.5. Synthesis of (MeCF$_3$)Rh(CO), **5**

2.5.5.1. Method A. Heating mixture of 0.133 g (0.347 mmol) H($MeCF_3$) and 0.0896 g (0.347 mmol) $Rh(CO)_2$(acac) in 15 mL acetone for 72 h, then removing volatiles under vacuum left a brown solid. The pentane soluble product was extracted from the brown solid by extractions with three 8 mL portions of pentane. Pentane was removed from the collected filtrates to give 0.162 g (91%) of pure **5** as a yellow solid.

2.5.5.2. Method B. In a manner similar to complex **1**, a mixture of 1.098 g (2.87 mmol) H($MeCF_3$), 2.9 mmol (1.8 mL of a 1.6 M solution in hexane) Li(*n*-Bu), and 0.557 g (1.43 mmol) of $[(CO)_2Rh(\mu\text{-}Cl)]_2$ in 15 mL THF gave 0.618 g (42%) of **5** as a yellow powder after organic work-up (extraction and crystallization). M.p.: 210–214 °C (dec.). Anal. Calcd. for $C_{21}H_{15}N_5F_3ORh$: C, 49.13; H, 2.95; N, 13.65. Found: C, 49.45; H, 3.04; N, 13.67. ^{1}H NMR (acetone-d_6): δ_H 8.64 (d, $J = 2$ Hz, 1H, H_3pz–$ArCF_3$), 8.52 (d, $J = 2$ Hz, 1H, H_3pz–tolyl), 7.89 (m, 1H, H_5pz–$ArCF_3$), 7.86 (m, 1H, H_5pz–tolyl), 7.76 (m, 1H, H_3–$ArCF_3$), 7.40 (m, 1H, H_3–tolyl), 7.28 (part of *AB*, 1H, $ArCF_3$), 7.10 (part of *AB*, 1H, $ArCF_3$), 7.00 (*AB* m, 2H, tolyl), 6.74 (dd, $J = 2$, 1 Hz, 1 H, H_4pz–$ArCF_3$), 6.70 (dd, $J = 2$, 1Hz, 1H, H_4pz–tolyl), 2.30 (s, 3H, $ArCH_3$) ppm. ^{13}C NMR (acetone-d_6): δ_C 192.4 (d, $^1J_{Rh-C} = 72$ Hz, CO), 150.0, 147.2 (d, $^3J_{Rh-C} = 3$Hz), 147.0 (d, $^3J_{Rh-C} = 3$Hz), 141.8, 131.3, 131.2, 131.1, 131.0, 130.4, 130.1, 129.5 (d, $^3J_{Rh-C} = 1$Hz), 125.8 (q, $^1J_{C-F} = 272$ Hz, CF_3), 125.4 (q, $^3J_{C-F} = 4$ Hz), 124.5, 124.0, 122.3, 121.0 (q, $^3J_{C-F} = 4$ Hz), 117.5 (q, $^2J_{C-F} = 33$ Hz), 109.3 (d, $^3J_{Rh-C} = 2$Hz, C_4pz), 109.0 (d, $^3J_{Rh-C} = 2$ Hz, C_4pz), 20.5 ppm. ^{19}F NMR (acetone-d_6): δ_F −61.21 ppm. IR (ν_{CO}, cm^{-1}): 1958 (KBr pellet); 1962 (acetone).

LRMS (Direct Probe, *m/z*) (int.) [assign.]: 513 (11) $[LRh(CO)]^{\bullet+}$, 485 (26) $[LRh]^{\bullet+}$, 383 (100) $[HL]^{+}$.

2.5.6. Synthesis of $(CF_3CF_3)Rh(CO)$, **6**

2.5.6.1. Method A. A mixture of 0.119 g (0.272 mmol) $H(CF_3CF_3)$ and 0.0701 g (0.272 mmol) $Rh(CO)_2(acac)$ in 15 mL acetone was heated at reflux under nitrogen for 20 h to give 0.145 g (94%) of pure **6** as a yellow crystalline solid after removing solvent and H(acac) by vacuum distillation.

2.5.6.2. Method B. In a manner similar to that for compound **1**, 0.908 g (2.08 mmol) $H(CF_3CF_3)$, 2.1 mmol Li(*n*-Bu) (1.3 mL, 1.6 M in hexane) and 0.404 g (1.04 mmol) $[(CO)_2Rh(\mu\text{-}Cl)]_2$ in 30 mL THF gave 0.613 g (52%) of **6** as a yellow powder after work-up. M.p.: 250–254 °C (dec.) Anal. Calcd. for $C_{21}H_{12}N_5F_6ORh$: C, 44.47; H, 2.14; N, 12.35. Found: C, 44.97; H, 2.32; N, 11.95. ^1H NMR (acetone-d_6): δ_H 8.71 (d, $J = 2$ Hz, 2H, H_3pz), 7.93 (m, 2H, Ar-H), 7.87 (d, $J = 2$ Hz, 2H, H_5pz), 7.40 (part of *AB*, 1H, Ar-H), 7.26 (part of *AB*, 1H, Ar-H), 7.24 (s, 1H, Ar-H), 6.77 (t, $J = 2$, 2H, H_4pz) ppm. ^{13}C NMR (acetone-d_6): δ_C 192.0 (d, $^1J_{Rh-C} = 72$ Hz, CO), 148.7, 147.6 (d, $^3J_{Rh-C} = 3$ Hz), 131.9, 130.7, 125.8 (q, $^3J_{CF} = 3$ Hz), 125.2 (q, $^1J_{C-F} = 272$ Hz, CF_3), 123.9, 121.4 (q, $^3J_{C-F} = 4$ Hz), 120.3 (q, $^2J_{CF} = 33$ Hz), 109.5(d, $^3J_{Rh-C} = 2$ Hz, C_4pz) ppm. ^{19}F NMR (acetone-d_6): δ_F −61.64 ppm. IR (ν_{CO}, cm^{-1}): 1962 (KBr pellet); 1968 (acetone). LRMS (Direct Probe, *m/z*) (int.) [assign.]: 567 (38) $[LRh(CO)]^{\bullet+}$, 539 (100) $[LRh]^{\bullet+}$, 437 (8) $[HL]^{+}$.

2.6. Oxidative addition reactions with 1–6

2.6.1. Spectroscopic experiments (kinetics study): general considerations

Typical procedure for NMR scale experiments is as follows. About 4–6 mg of rhodium(I) complex, (^{R}ZX)Rh(CO), was added to a pre-weighed NMR tube and the mass of tube and sample are recorded. Next, 0.35 mL of acetone-d_6 was added to dissolve the rhodium complex. The tube was inserted into the spectrometer was allowed to equilibrate at the desired temperature (313–323 K) for 15 min. The tube was ejected from the spectrometer and an appropriate amount (5–10 μL, ≥10 mol equiv) of MeI or EtI was added by syringe and rapidly returned to the heated spectrometer (representing the reference time of 0 s). The NMR spectra were recorded after 5 min, then after 10 min intervals thereafter. While no problems were encountered in obtaining ^{13}C NMR spectra for reactions involving MeI, the spectra from reactions using EtI did not give useful signal-to-noise ratios due to extensive decomposition that occurred during overnight acquisitions (exacerbated by the long reaction times). Therefore, ^{13}C NMR data are only reported for MeI cases. Only representative data for reactions involving (MeMe)Rh(CO) are given below, those for the remaining derivatives can be found in the main text and the Supplementary data.

(MeMe)Rh(Me)(CO)(I), **7_{Me}**. ^1H NMR (acetone-d_6): δ_H 8.55 (d, $J = 3$ Hz, 2H, H_3pz), 8.07 (d, $J = 2$ Hz, 1H, H_5pz), 7.90 (d, $J = 2$ Hz, 1H, H_5pz), 7.43 (s, 1H, Ar), 7.33 (s, 1H, Ar), 7.16 (part of *AB*, $J_{app} = 8$ Hz, 1H, Ar), 7.05 (part of *AB*, $J_{app} = 8$ Hz, 1H, Ar), 6.93 (part of *AB*, $J_{app} = 8$, 2 Hz, 1H, Ar), 6.86 (part of *AB*, $J_{app} = 8$, 2 Hz, 1H, Ar), 6.77 (t, $J = 3$ Hz, 1H, H_4pz), 6.76 (t, $J = 3$ Hz, 1H, H_4pz), 2.28 (s, 3H, $ArCH_3$), 2.27 (s, 3H, $ArCH_3$), 1.26 (d, $^2J_{Rh-H} = 2$ Hz, 3H, Rh−CH_3) ppm. ^{13}C NMR (acetone-d_6): δ_C 187.4 (d, $^1J_{Rh-C} = 55$ Hz, Rh−CO), 149.1, 145.2 (d, $^3J_{Rh-C} = 1$ Hz), 145.1, 142.3, 132.8, 131.8, 131.6, 130.4, 129.6, 129.1, 128.9, 128.8, 128.6, 126.2, 125.1, 122.9, 122.7, 109.8 (C_4pz), 109.3(C_4pz), 20.6, 20.5, 9.9 ($J_{Rh-C} = 20$ Hz, $RhCH_3$) ppm. IR (acetone, ν_{CO}, cm^{-1}): 2063. LRMS (ESI(+), *m/z*) (int.) [assign.]: 446 (13) $[LRh(Me)]^{+}$, 474 (100) $[LRh(Me)(CO)]^{+}$, 487 (20) $[LRh(Me)(CH_3CN)]^{+}$, 515 (67) $[LRh(Me)(CO)(CH_3CN)]^{+}$, 601 (3) $[LRh(Me)(CO)(I)]^{\bullet+}$, 927 (1) $[L_2Rh_2(Me)_2Cl]^{+}$, 955 (2) $[L_2Rh_2(Me)_2(CO)Cl]^{+}$, 983 (7) $[L_2Rh_2(Me)_2(CO)_2Cl]^{+}$, 1019 (2) $[L_2Rh_2(Me)_2I]^{+}$, 1047 (2) $[L_2Rh_2(Me)_2(CO)I]^{+}$, 1075 (15) $[L_2Rh_2(Me)_2(CO)_2I]^{+}$.

(MeMe)Rh(Et)(CO)(I), **7_{Et}**. ^1H NMR (acetone-d_6): δ_H 8.53 (m, 2H, H_3pz), 8.06 (d, $J = 2$ Hz, 1H, H_5pz), 7.97 (d, $J = 2$ Hz, 1H, H_5pz), 7.46 (s, 1H, Ar), 7.28 (s, 1H, Ar), 7.19 (part of *AB*, $J_{app} = 8$ Hz, 1H, Ar), 7.04 (part of *AB*, $J_{app} = 8$ Hz, 1H, Ar), 6.95 (part of *AB*, 1H, Ar), 6.84 (part of *AB*, 1H, Ar), 6.77 (t, $J = 2$ Hz, 1H, H_4pz), 6.75 (t, $J = 2$ Hz, 1H, H_4pz), 2.44 (m, 1H, CH_2), 2.31 (s, 3H, Ar-CH_3), 2.27 (s, 3H, $ArCH_3$), 2.23 (m, 1H, CH_2), 0.65 (td, $^2J_{C-H} = 8$ Hz, $^3J_{Rh-H} = 1$ Hz, 3H, $EtCH_3$) ppm. IR (acetone, ν_{CO}, cm^{-1}): 2055. HRMS [ESI(+), *m/z*] Calcd. (Obs) for $C_{25}H_{27}N_5Rh$, $[LRh(Et)(CO)]^{+}$, 516.1271 (516.1276). LRMS (ESI(+), *m/z*) (int.) [assign.]: 432 (6) $[LRh(H)]^{+}$, 446 (58) $[LRh(Et)]^{+}$, 472 (14) $[LRh(CH_3CN)]^{+}$, 488 (100) $[LRh(Et)(CO)]^{+}$, 501 (35) $[LRh(Et)(CH_3CN)]^{+}$, 529 (4) $[LRh(Et)(CO)(CH_3CN)]^{+}$, 615 (1) $[LRh(Et)(CO)(I)]^{\bullet+}$, 927 (0.2) $[L_2Rh_2(Et)_2Cl]^{+}$, 955 (0.5) $[L_2Rh_2(Et)_2(CO)Cl]^{+}$, 1011 (5) $[L_2Rh_2(Et)_2(CO)_2Cl]^{+}$, 1019 (0.1) $[L_2Rh_2(Et)_2I]^{+}$, 1047 (0.5) $[L_2Rh_2(Et)_2(CO)I]^{+}$, 1103 (9) $[L_2Rh_2(Et)_2(CO)_2I]^{+}$.

2.6.2. Synthesis of (MeMe)Rh(Me)(CO)(I), 7_{Me}.

A 0.15 mL (2.4 mmol) aliquot of CH_3I was added by syringe to a yellow solution of 0.109 g (0.238 mmol) **1** in 15 mL acetone. After the resulting red solution had been stirred at room temperature for 10 min, volatiles were removed under vacuum to give 0.109 g (76%) of **7_{Me}** as red-orange microcrystalline powder. M.p.: 245–250 °C, (dec). Anal. Calcd for $C_{22}H_{21}N_5IORh$: C, 43.95; H, 3.52; N, 11.65. Found: C, 44.13; H, 3.29; N, 11.92. ^1H NMR (CD_2Cl_2): δ_H 8.13 (d, $J = 2$ Hz, 1H, H_5pz), 8.12 (d, $J = 2$ Hz, 1H, H_5pz), 8.02 (d, $J = 1$ Hz, 1H, H_3pz), 7.52 (d, $J = 1$ Hz, 1H, H_3pz), 7.22–7.12 (overlapping s's and part of *AB*, 4 H, Ar), 6.92 (part of *AB*, 2H, Ar), 6.66 (d, $J = 2$ Hz, 1H, H_4pz), 6.65 (d, $J = 2$ Hz, 1H, H_4pz), 2.34 (s, 3H, $ArCH_3$), 2.30 (s, 3H, $ArCH_3$), 1.25 (d, $^2J_{Rh-H} = 2$ Hz, 3H, Rh−CH_3). IR (ν_{CO}, cm^{-1}): 2060 (KBr pellet).

2.6.3. Synthesis of (MeMe)Rh(I)$_2$(CO), 7_I.

A solution of 0.0262 g (0.103 mmol) I_2 in 15 mL acetone was added dropwise via cannula to a solution of 0.0474 g (0.103 mmol) **1** in 10 mL acetone. After the resulting green-brown solution had been stirred at room temperature for 12 h, acetone was removed under vacuum to give 0.0739 g (100%) of **7_I** as dark yellow-brown powder. M.p.: >300 °C. Anal. Calcd. for $C_{21}H_{18}N_5OI_2Rh$: C, 35.37; H, 2.54; N, 9.82. Found: C, 35.55; H, 2.61; N, 10.13. ^1H NMR (acetone-d_6): 8.62 (d, $J = 3$ Hz, 2H, H_3pz), 8.08 (d, $J = 3$ Hz, 2H, H_5pz), 7.40 (s, 2H, Ar), 7.16 (part of *AB*, $J_{app} = 8$ Hz, 2H, Ar), 6.93 (part of *AB*, $J_{app} = 8$, 1 Hz, 2H, Ar), 6.81 (t, $J = 3$, 2H, H_4pz), 2.30 (s, 6H, $ArCH_3$). ^{13}C NMR (acetone-d_5): 206.1 (d, $^1J_{Rh-C} = 40$ Hz, Rh−CO), 149.9 (d, $^3J_{Rh-C} = 1$ Hz), 145.1, 132.9, 132.5, 129.3, 129.1, 126.0, 122.7, 109.9 (d, $^3J_{Rh-C} = 1$ Hz, C_4pz), 20.6. ^1H NMR (CD_2Cl_2): 8.16 (d, $J = 3$ Hz, 2H, H_3pz), 7.89 (d, $J = 2$ Hz, 2H, H_5pz), 7.21 (part of *AB*, $J_{app} = 8$ Hz, 2H, Ar), 7.17 (s, 2H, Ar), 6.95 (part of *AB*, $J_{app} = 8$, 1 Hz, 2H, Ar), 6.67 (dd, $J = 3$, 2 Hz, 2H, H_4pz), 2.34 (s, 6H, $ArCH_3$). IR (ν_{CO}, cm^{-1}): 2080 (KBr pellet); 2078 (acetone). HRMS [ESI(+), *m/z*] Calcd. (Obs) for $C_{21}H_{18}I_2N_5ORh$, $[LRh(I)_2(CO)]^{\bullet+}$, 712.8656 (712.8652). LRMS (ESI(+), *m/z*) (int.) [assign.]: 713 (26) $[LRh(I)_2(CO)]^{\bullet+}$, 714 (100) $[HLRh(I)_2(CO)]^{+}$, 726 (12) $[LRh(I)(CH_3CN)]^{+}$.

2.6.4. Synthesis of mer, trans-[(MeMe)Rh(Me)(μ-I)]$_2$, 13_{Me}.

A mixture of 0.0420 g (91.4 μmol) **1** and 57.0 μL (91.6 mmol) CH_3I was left undisturbed for 2d at room temperature in a capped vial during which time small needles of insoluble product deposited. After 2 days the solution was decanted and the needles were washed with Et_2O and were dried under vacuum to give 0.0483 g (92%) of **13_{Me}** as a red crystalline solid. M.p.: >300 °C. Anal. Calcd. for $C_{21}H_{21}N_5IRh$: C, 44.00; H, 3.69; N, 12.22. Found: C, 44.03; H, 3.74; N, 11.99. HRMS [ESI(+), *m/z*] Calcd. (Obs) for $C_{42}H_{42}IN_{10}Rh_2$, $[L_2Rh_2(Me)_2(I)]^{\bullet+}$, 1019.0749 (1019.0731). LRMS (ESI(+), *m/z*) (int.) [assign.]: 446 (25) $[LRh(Me)]^{+}$, 487 (100) $[LRh(Me)(CH_3CN)]^{+}$, 528 (6) $[LRh(Me)(CH_3CN)_2]^{+}$, 573 (27) $[LRh(Me)(I)]^{\bullet+}$, 727 (1.5) $[HLRh(I)_2(CH_3CN)]^{+}$, 927 (0.7) $[L_2Rh_2(Me)_2Cl]^{+}$, 968 (0.7)

$[L_2Rh_2(Me)_2(CH_3CN)Cl]^+$, 1019 (5) $[L_2Rh_2(Me)_2I]^+$, 1060 (6) $[L_2Rh_2(Me)_2(CH_3CN)(I)]^+$, 1101 (2) $[L_2Rh_2(Me)_2(CH_3CN)_2(I)]^+$, 1131 (0.7) $[L_2Rh_2(Me)(I)_2]^{\bullet+}$, 1146 (0.7) $[L_2Rh_2(Me)_2(I)_2]^{\bullet+}$, 1172 (1.1) $[L_2Rh_2(Me)_2(CH_3CN)(I)_2]^{\bullet+}$, 1187 (0.6) $[L_2Rh_2(Me)_2(CH_3CN)_2(I)_2]^{\bullet+}$. An X-ray-quality single crystal was selected from another similar preparation, but before decanting the mother liquor. This crystal showed about 9.37% replacement of iodide for each of the methyls, or equivalently represents a mixture of 90.63% **13_{Me}** and 9.37% **13_I**. Given the combustion analysis data, this crystal is likely not representative of the bulk.

*2.6.5. Synthesis of mer, trans-[(MeMe)Rh(I)(μ-I)]$_2$, **13_I**·Et$_2$O*

A solution of 0.0524 g (0.206 mmol) I_2 in 15 mL THF was added to a solution of 0.0948 g (0.206 mmol) **1** in 5 mL THF. The resulting red-brown solution was heated at reflux for 12 h. After cooling to room temperature, the precipitate was collected by filtration, washed with 5 mL each THF and Et_2O and then was dried under vacuum to give 0.110 g (74%) of **13_I**·Et_2O as an orange-brown solid. M.p.: >300 °C. Anal. Calcd. for $C_{44}H_{46}N_{10}I_4ORh_2$, **$13_I$**·$Et_2O$: C, 36.59; H, 3.21; N, 9.70. Found: C, 36.34; H, 2.98; N, 9.27. LRMS (ESI(+), *m*/*z*) (int.) [assign.]: 466 (12) $[LRh(Cl)]^+$, 476 (3) $[LRh(formate)]^+$, 517 (10) $[LRh(formate)(CH_3CN)]^+$, 531 (21) $[LRh(CH_3CO_2)(CH_3CN)]^+$, 548 (9) $[LRh(formate)(CH_3CN)_2]^+$, 558 (55) $[LRh(I)]^+$, 599 (60) $[LRh(I)(CH_3CN)]^+$, 640 (100) $[LRh(I)(CH_3CN)_2]^+$, 686 (5) $[HLRh(I)_2]^+$, 726 (43) $[LRh(I)_2(CH_3CN)]^{\bullet+}$, 1243 (1) $[L_2Rh_2(I)_3]^+$, 1261 (0.3) $[L_2Rh_2(I)_3(H_2O)]^+$, 1284 (2) $[L_2Rh_2(I)_3(CH_3CN)]^+$, 1325 (1) $[L_2Rh_2(I)_3(CH_3CN)_2]^+$. X-ray quality crystals were obtained by vapor diffusion of Et_2O into a room temperature solution that was obtained by mixing 0.103 mmol of each **1** and I_2 in 2 mL THF.

3. Single crystal X-ray crystallography

X-ray intensity data from a yellow needle of **1** and a yellow block of **5** were collected at 273 K with a Bruker AXS 3-circle diffractometer equipped with a SMART2 [35] CCD detector using Mo(Kα) for the former and Cu(Kα) radiation for the latter. X-ray intensity data from a yellow needle of **2**·C_6H_6, a yellow prism of **3**, a yellow prism of **4**·C_6H_6, a brown prism of **7_{Et}**, a brown prism of **7_I**·1.5acetone, an orange prism of **8_{Me}**·**C_6H_6**, a brown prism of **13_{Me}**·acetone, and a brown needle of **13_I**·Et_2O were measured with an Oxford Diffraction Ltd. Supernova diffractometer equipped with a 135 mm Atlas CCD detector using Mo(Kα) for all except **3** and **4**·C_6H_6 which used Mo(Kα) radiation. Raw data frame integration and Lp corrections were performed with either CrysAlis Pro (Oxford Diffraction, Ltd.) [36] or SAINT+ (Bruker) [35]. Final unit cell parameters were determined by least-squares refinement of 9874, 13022, 10797, 9932, 9989, 28084, 20898, 11437, 15332, and 9630 reflections from the data sets of **1**, **2**·C_6H_6, **3**, **4**·C_6H_6, **5**, **7_{Et}**, **7_I**·1.5acetone, **8_{Me}**·C_6H_6, **13_{Me}**·acetone, **13_I**·Et_2O, respectively, with $I > 2\sigma(I)$ for each. Analysis of the data showed negligible crystal decay during collection in each case. Direct methods structure solutions, difference Fourier calculations and full-matrix least-squares refinements against F^2 were performed with SHELXTL [37]. Numerical absorption corrections and based on the real shape of the crystals were applied with SADABS for **1** and **5** [35]. Empirical absorption corrections were applied to the data of **2**·C_6H_6 and **8_{Me}**·C_6H_6 using spherical harmonics implemented in the SCALE3 ABSPACK multi-scan method [38]. Numerical absorption corrections based on gaussian integration over a multi-faceted crystal model were applied to the data of the remaining complexes. All non-hydrogen atoms were refined with anisotropic displacement parameters. Hydrogen atoms were placed in geometrically idealized positions and included as riding atoms. The X-ray crystallographic parameters and further details of data collection and structure refinements are presented in Tables 1–4. The crystal of **5** is a quasi-merohedral pseudo-orthorhombic TWIN with 27% contribution of a (−1000 to 10001) component where the CF_3 and CH_3 groups in both symmetrically independent molecules are interchangeably superimposed. The CF_3 group has an apparent rotational disorder; however, given the low population against the superimposed Me-group, we treated this group adequately with an anisotropic representation and avoided over-modeling by splitting it into two different orientations.

Table 1
Crystallographic data collection and structure refinement for **1**, **2**, and **3**.

Compound	**1**	**2**·C_6H_6	**3**
Formula	$C_{21}H_{18}N_5ORh$	$C_{29}H_{28}N_5ORh$	$C_{27}H_{30}N_5ORh$
Formula weight	459.31	565.47	543.47
Crystal system	Orthorhombic	Triclinic	Triclinic
Space group	*Pnna*	*P*−1	*P*−1
Temp. [K]	100(2)	100.0	100(2)
a [Å]	9.7817(7)	10.0029(3)	12.4341(5)
b [Å]	26.5319(18)	10.9129(4)	13.6245(7)
c [Å]	14.2307(10)	12.7569(4)	14.8775(6)
α [°]	90	74.557(3)	84.671(4)
β [°]	90	72.389(3)	86.420(3)
γ [°]	90	87.204(3)	76.703(4)
V [Å^3]	3693.3(4)	1278.60(7)	2440.01(18)
Z	8	2	4
$D_{calcd.}$ [g cm^{-3}]	1.652	1.469	1.479
λ [Å] (Mo or Cu Kα)	0.71073	0.71073	1.5418
μ.[mm^{-1}]	0.947	0.699	5.888
Abs. Correction	Numerical	Multi-scan	Numerical
F(000)	1856	580	1120
2θ range [°]	3.08 to 64.18	6.78 to 59.16	6.68 to 147.62
Reflections collected	61457	22593	23525
Independent reflections	6291[*R*(int) = 0.0384]	6410[*R*(int) = 0.0324]	9614[*R*(int) = 0.0318]
T_min/max	0.6906/0.9255	0.95436/1.00000	0.598/0.815
Data/restraints/parameters	6291/0/259	6410/0/329	9614/0/625
Goodness-of-fit on F^2	0.998	1.071	1.022
*R*1/*wR*2[$I > 2\sigma(I)$][a]	0.0237/0.0565	0.0278/0.0569	0.0254/0.0646
*R*1/*wR*2 (all data)[b]	0.0320/0.0609	0.0343/0.0604	0.0303/0.0673
Largest diff. peak/hole/e Å^{-3}	0.901/−0.392	0.657/−0.440	0.710/−0.537

[a] $R = \Sigma||F_o|-||F_c||/\Sigma|F_o|$.
[b] $wR = [\Sigma w(|F_o^2|-|F_c^2|)^2/\Sigma w|F_o^2|^2]^{1/2}$.

Table 2
Crystallographic data collection and structure refinement for **4**·C_6H_6, **5**, and $\mathbf{7_{Et}}$.

Compound	**4**·C_6H_6	**5**	$\mathbf{7_{Et}}$
Formula	$C_{26}H_{22}N_5ORh$	$C_{21}H_{15}F_3N_5ORh$	$C_{23}H_{23}IN_5ORh$
Formula weight	523.40	513.29	615.27
Crystal system	Triclinic	Monoclinic	Monoclinic
Space group	*P*−1	$P2_1/n$	$P2_1/n$
Temp. [K]	101.0	100.4	100.0
a [Å]	9.0197(3)	9.9482(3)	7.44834(10)
b [Å]	10.0599(3)	26.7919(9)	18.3451(3)
c [Å]	12.7565(4)	14.5872(5)	16.7515(2)
α [°]	83.830(2)	90.00	90.00
β [°]	81.875(3)	90.2190(10)	92.4100(12)
γ [°]	77.668(3)	90.00	90.00
V [Å^3]	1115.86(6)	3887.9(2)	2286.90(6)
Z	2	8	4
$D_{calcd.}$ [g cm^{-3}]	1.558	1.754	1.787
λ [Å] (Mo or Cu Kα)	0.7107	1.54178	0.7107
μ.[mm^{-1}]	0.795	7.585	2.122
Abs. Correction	Numerical	Numerical	Numerical
F(000)	532	2048	1208
2θ range [°]	6.84 to 59.16	6.06 to 136.24	7.06 to 59.06
Reflections collected	25073	7008	60084
Independent reflections	5708[*R*(int) = 0.0322]	6843[*R*(int) = 0.0000]	6156[*R*(int) = 0.0332]
T_min/max	0.917/0.975	0.2826/0.3998	0.616/0.746
Data/restraints/parameters	5708/0/299	6843/24/621	6156/0/283
Goodness-of-fit on F^2	1.075	1.034	1.053
*R*1/*wR*2[$I > 2\sigma(I)$][a]	0.0382/0.0907	0.0404/0.0976	0.0190/0.0390
*R*1/*wR*2 (all data)[b]	0.0446/0.0950	0.0415/0.0981	0.0235/0.0410
Largest diff. peak/hole/e Å−3	1.758/−1.519	0.824/−0.826	0.467/−0.602

[a] $R = \Sigma||F_o|-||F_c||/\Sigma|F_o|$.
[b] $wR = [\Sigma w(|F_o^2|-|F_c^2|)^2/\Sigma w|F_o^2|^2]^{1/2}$.

4. Results and discussion

4.1. Syntheses

The synthetic routes to the six NNN-pincer ligands used in this study are given in Scheme 1. The syntheses of the di[(2-3R-pyrazolyl)-*p*-tolyl]amine ligands (R = H, Me, ^{i}Pr), H(^{R}MeMe), have been detailed elsewhere [34]. Briefly, H(^{R}MeMe) can be prepared in about 65% yield (after two steps) by first bromination of the commercially-available ditolylamine followed by a CuI-catalyzed amination reaction with the appropriate 3R-pyrazole [39]. After significant synthetic effort, an optimized convergent route to ligands decorated with two different pyrazolylaryl arms, H(MeH) and H($MeCF_3$), and a ligand with two trifluoromethylaryls, H(CF_3CF_3), was discovered

Table 3
Crystallographic data collection and structure refinement for $\mathbf{7_I}$·1.5acetone and $\mathbf{8_{Me}}$·C_6H_6.

Compound	$\mathbf{7_I}$·1.5acetone	$\mathbf{8_{Me}}$·C_6H_6
Formula	$C_{25.5}H_{27}I_2N_5O_{2.5}Rh$	$C_{30}H_{31}IN_5ORh$
Formula weight	800.23	707.41
Crystal system	Triclinic	Monoclinic
Space group	*P*−1	$P2_1/c$
Temp. [K]	100.3	100.3
a [Å]	13.0548(4)	9.4775(2)
b [Å]	13.9045(4)	22.6275(5)
c [Å]	15.7643(4)	13.5609(4)
α [°]	83.791(2)	90.00
β [°]	79.004(2)	100.519(3)
γ [°]	85.109(2)	90.00
V [Å^3]	2786.41(13)	2859.30(12)
Z	4	4
$D_{calcd.}$ [g cm^{-3}]	1.908	1.643
λ [Å] (Mo or Cu Kα)	0.7107	0.7107
μ.[mm^{-1}]	2.862	1.709
Abs. Correction	Numerical	Multi-scan
F(000)	1544	1408
2θ range [°]	6.6 to 59.22	6.84 to 59.1
Reflections collected	53463	32496
Independent reflections	14130[*R*(int) = 0.0334]	7333[*R*(int) = 0.0406]
T_min/max	0.608/0.898	0.85935/1.00000
Data/restraints/parameters	14130/0/659	7333/0/348
Goodness-of-fit on F^2	1.059	1.113
*R*1/*wR*2[$I > 2\sigma(I)$][a]	0.0268/0.0509	0.0333/0.0633
*R*1/*wR*2 (all data)[b]	0.0380/0.0564	0.0499/0.0745
Largest diff. peak/hole/e Å^{-3}	1.559/−1.098	1.543/−0.799

[a] $R = \Sigma||F_o|-||F_c||/\Sigma|F_o|$.
[b] $wR = [\Sigma w(|F_o^2|-|F_c^2|)^2/\Sigma w|F_o^2|^2]^{1/2}$.

Table 4
Crystallographic data collection and structure refinement for $\mathbf{13_{Me}}$·acetone, and $\mathbf{13_I}$·Et_2O.

Compound	$\mathbf{13_{Me}}$·acetone	$\mathbf{13_I}$·Et_2O
Formula	$C_{44.81}H_{47.44}I_{2.19}N_{10}ORh_2$	$C_{44}H_{46}I_4N_{10}ORh_2$
Formula weight	1225.52	1444.33
Crystal system	Monoclinic	Monoclinic
Space group	$P2_1/n$	$P2_1/n$
Temp. [K]	100.0	100.7
a [Å]	15.7695(3)	16.2250(5)
b [Å]	8.12639(17)	8.4566(2)
c [Å]	20.1709(4)	19.2983(6)
α [°]	90.00	90.00
β [°]	93.007(2)	93.683(3)
γ [°]	90.00	90.00
V [Å^3]	2581.33(9)	2642.42(13)
Z	2	2
$D_{calcd.}$ [g cm^{-3}]	1.577	1.815
λ [Å] (Mo or Cu Kα)	0.7107	0.7107
μ.[mm^{-1}]	1.988	3.002
Abs. Correction	Numerical	Numerical
F(000)	1200	1380
2θ range [°]	6.72 to 59.08	6.78 to 59.06
Reflections collected	32699	40194
Independent reflections	6684[*R*(int) = 0.0296]	6940[*R*(int) = 0.0585]
T_min/max	0.607/0.926	0.731/0.975
Data/restraints/parameters	6684/6/302	6940/7/300
Goodness-of-fit on F^2	1.107	1.049
*R*1/*wR*2[$I > 2\sigma(I)$][a]	0.0283/0.0859	0.0497/0.1218
*R*1/*wR*2 (all data)[b]	0.0340/0.0896	0.0787/0.1380
Largest diff. peak/hole/e Å^{-3}	1.349/−0.452	1.696/−1.114

[a] $R = \Sigma||F_o|-||F_c||/\Sigma|F_o|$.
[b] $wR = [\Sigma w(|F_o^2|-|F_c^2|)^2/\Sigma w|F_o^2|^2]^{1/2}$.

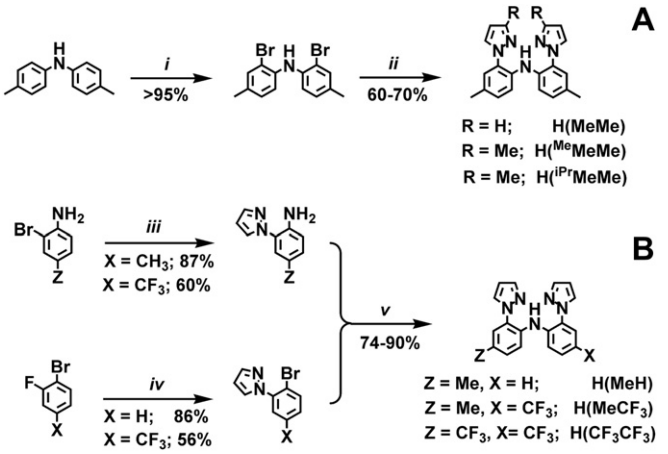

Scheme 1. Summary of preparative routes to the NNN-pincer ligands used in this work. Key: i) Br_2, 1:1 CH_2Cl_2:MeOH 0 °C; ii) 3.5 equiv. Hpz, xs K_2CO_3, cat. CuI, cat. DMED, xylenes, reflux 24 h; iii) 1.1 Hpz, 1.2 Cs_2CO_3, cat. CuI, DMF; iv) NaH, Hpz, DMF, Δ 30 min; v) cat. CuI, 1.2 Cs_2CO_3, dioxane, Δ 16 h.

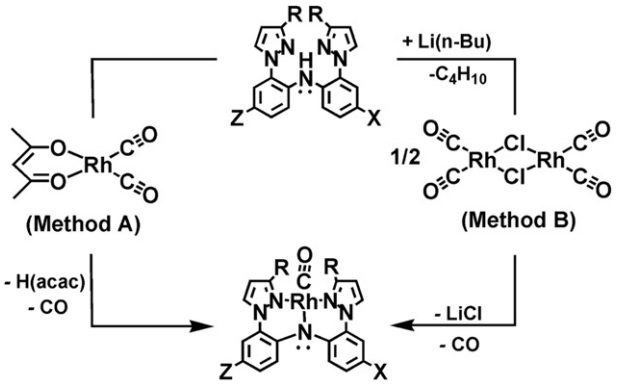

(L)Rh(CO) L = (^{R}ZX), (#)	Method A	Method B	ν_{CO} (cm^{-1}) acetone
MeMe, (1)	95%	42%	1955
^{Me}MeMe, (2)	75%	25%	1951
^{iPr}MeMe, (3)	45%*	37%	1948
MeH, (4)	84%	na	1956
$MeCF_3$, (5)	91%	42%	1962
CF_3CF_3, (6)	76%	32%	1968

na, not attempted

Scheme 2. Preparation of carbonylrhodium(I) pincer complexes. (*yield from NMR spectroscopic measurement, not isolated).

(Scheme 1B) that permitted fine-tuning of the electronic properties of the ligands. In this approach, each 'arm' of the appropriate ligand was constructed separately before being assembled together in a final step that employs a CuI-catalyzed amination reaction. That is, the appropriate commercially-available *para*-X-anilines (X = CF_3 or CH_3) were quantitatively *ortho*-brominated with NBS in CH_3CN at 0 °C, then a CuI-catalyzed amination reaction of the 2-bromo-4-X-anilines and pyrazole gave the corresponding 2-pyrazolyl-4-X-aniline "arm" in good yield [34]. The second 'arm' of the pincer ligand is prepared by a nucleophilic substitution reaction between sodium pyrazolide (prepared in-situ from NaH and Hpz) and commercially-available 1-bromo-2-fluorobenzene or 1-bromo-2-fluoro-4-(trifluoromethyl)benzene in DMF. In the final step, the two separate arms are attached by a second, convenient amination reaction that employed 20 mol % CuI as a catalyst, 1.2 equiv Cs_2CO_3 as a base, and dioxane as a solvent. The use of this CuI catalyst system circumvented the need for expensive palladium catalysts and chelating phosphine co-catalysts (Xanthphos, DPEPhos, etc.) that gave lower yields of H($MeCF_3$) and H(CF_3CF_3) after longer periods of time. The possibility of using a lower catalyst loading was not investigated due to the success of the reactions and the low cost of CuI. Alternative preparative routes using various Ullman-type conditions (Cu^0 powder, Ph_2O, high temp > 200 °C) were low-yielding (15–25%) and gave significant amounts of 2,2′-pz_2biaryls as by-products. Furthermore, a direct route to H($MeCF_3$) and H(CF_3CF_3) similar to that for H(^{R}MeMe) was hampered by a number of factors, including: i) diarylamines with *para*-trifluoromethyl-substituents were neither commercially-available nor well-known; ii) once in hand, the final coupling reaction between di(2-bromoaryl)amines and pyrazole (in xylene with K_2CO_3 and DMED) was often very sluggish, incomplete, and accompanied by unexpected decomposition or by-products including those derived from C–F activation [40].

Since the deprotonated, anionic NNN-pincer ligands (^{R}ZX)$^-$ are six-electron donors in the ionic formalism (or five electron donors in the covalent formalism), square planar, sixteen-electron complexes of the type (^{R}ZX)Rh(CO) were the anticipated products from known carbonylrhodium(I) reagents.

Scheme 2 outlines the two successful synthetic routes that were used for the preparation of the six new carbonylrhodium(I) complexes, **1**–**6**.

First, **1**–**6** could be obtained by an acetylacetone elimination route between the desired ligand and $Rh(CO)_2$(acac). The metathetical reactions between $[Rh(CO)_2(\mu\text{-}Cl)]_2$ and "Li(^{R}ZX)" (prepared in-situ from the ligand and Li(*n*-Bu) at low temperature in THF, or in toluene for **3**) were also used to access all but **4**, which was not attempted. For complexes **1**, **2**, **5**, and **6**, the acetylacetone elimination route is superior to the metathesis route because the former goes to completion (by NMR monitoring) and the separation of the desired products and byproducts is simpler; neither was true for **3**. For complex **3**, low yields were obtained by either route; however, the metathetical reaction using toluene as a solvent gave the best isolated yield because the product mixture was the easiest to separate by fractional precipitation from pentane. The low isolated yield of **3** by either route can be attributed to a number of factors. First, the acetylacetone elimination reaction is only about 45% complete after three days, and after such time significant free ligand, unreacted $Rh(CO)_2$(acac), and unidentified decomposition products are also found. Secondly, the high solubility of H(^{iPr}MeMe), **3**, and byproducts in most organic solvents complicates the separation of the complex from mixtures obtained by either route. Thirdly, the "Li(^{R}ZX)" salts appear to be temperature-sensitive in THF and to a lesser extent in toluene, indicated by the loss of their characteristic cyan luminescence upon UV irradiation (254 nm, see Supplementary data) when solutions are warmed above about −20 °C, which may contribute to the generally lower isolated yields of rhodium(I) products from the metathetical reactions.

Once isolated, the yellow complexes **1**–**6** appear air-stable as solids. Aerated solutions (hydrocarbon, ethereal, halocarbons, acetone or CH_3CN) of **1**–**6** are initially yellow but slowly darken and leave brown mirrors on the glassware. This decomposition occurs slowly over the course of week or two for solutions in nonpolar hydrocarbons (pentane, hexane, benzene) but occurs more quickly with increasing polarity of other solvents (a few minutes for CH_3CN solutions). Thus, spectroscopic data were acquired using freshly prepared yellow solutions of **1**–**6** that were protected from the atmosphere when possible.

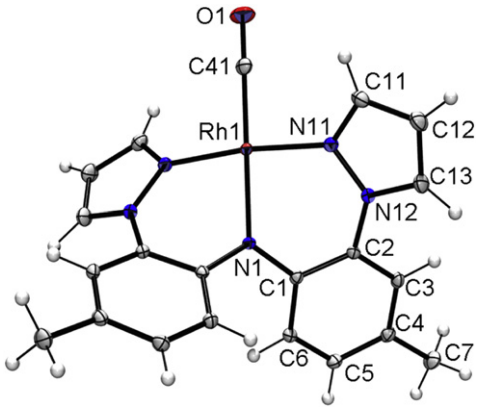

Fig. 2. Structure of (MeMe)Rh(CO), **1**. Selected bond distances (Å): Rh1–N1, 2.036(2); Rh1–N11, 2.024(1); Rh1–C41, 1.832(2); C41–O1, 1.148(3); Selected bond angles (°): N1–Rh1–C41 180.0; N11–Rh1–N11′, 173.08(7); N11–Rh1–N1, 86.54(3); C41–Rh1–N11, 93.46(3).

4.2. Description of crystal structures

Complexes **1**–**5** were characterized by single crystal X-ray diffraction that verified the anticipated monomeric nature of the complexes and the square planar geometry of donor atoms about rhodium. The molecular structures of **1** and **2** are given in Figs. 2 and 3, respectively, others are provided in the Supplementary data.

In each structurally characterized complex, the RhN_3C kernel adopts a distorted square planar geometry (sum of angles about rhodium = 360°) where the two acute N11–Rh–N1 and N21–Rh–N1 angles (Fig. 3) give rise to non-linear ligating *trans*-pyrazolyl nitrogens, with N_{pz}–Rh–N_{pz} angles that range between 169.0(1)° for **3** to 173.8(2)° for **5**. The rhodium–nitrogen(pyrazolyl), Rh–N_{pz}, bond distances increase slightly with increasing steric bulk of the 3-pyrazolyl substituent. Thus, the average Rh–N_{pz} distances of 2.025(1) Å and 2.028(6) Å (for two independent units) in each **1** and **5**, respectively, are comparable to or shorter than 2.035(2) Å for **2** which in turn is shorter than that of 2.055(2) Å in **3**. All of the Rh–N_{pz} bond distances in **1**–**5** are comparable to those found in $[EtN(CH_2pz^*)_2]Rh(CO)]^+$ (pz^* = 3,5-dimethylpyrazolyl, avg 2.019(3) Å) [41], $\{[O(CH_2pz^*)_2]Rh(CO)\}^+$ (avg 2.037(4) Å) [42], or $\{[S(CH_2CH_2pz^*)_2]Rh(CO)\}^+$ (avg 2.044(2) Å) [43]. The remaining bond distances for the rhodium-amido (Rh–N1 ranging from 2.027(2) Å in **1** and 2.050(4) Å in **5**) and rhodium carbonyl (Rh–C41 ranging from 1.812(6) Å in **5** to 1.834(2) Å in **3** and C41–O1 ranging from 1.147(2) Å in **3** to 1.170(8) Å in **5**) fragments in line with other carbonylrhodium(I) complexes of amido-anchored pincer complexes [19–22], [24] [44].

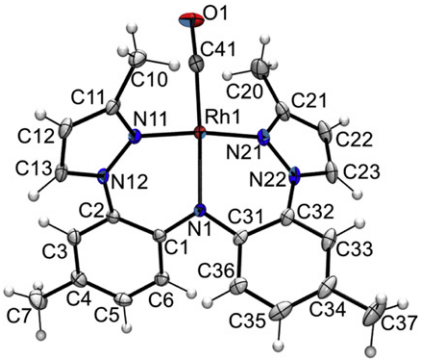

Fig. 3. Structure of (^{Me}MeMe)Rh(CO) in the crystal of **2**·C_6H_6. Selected bond distances (Å):. Rh1–N1, 2.039(2); Rh1–N11, 2.039(2); Rh1–N21, 2.032(2); Rh1–C41, 1.813(2); C41–O1, 1.154(3); Selected bond angles (°): N1–Rh1–C41 176.0(1); N11–Rh1–N21 173.2(1); N1–Rh1–N11, 86.7(1); N21–Rh1–N1, 86.6(1); C41–Rh1–N11, 94.9(1); C41–Rh1–N21, 91.9(1).

4.3. IR spectroscopic data

As expected for the series of complexes **1**, **4**, **5** and **6**, the frequency for the C–O stretching band in the IR spectrum of each complex increased with the extent that the electron-donating methyls were replaced by either hydrogen or by electron-withdrawing trifluoromethyl groups (ν_{CO} 1952 cm^{-1} for **1**, 1954 cm^{-1} for **4**, 1958 cm^{-1} for **5**, and 1962 cm^{-1} for **6** as KBr pellets). Although the number of data points is rather limited, there is a strong correlation between the energy of the C–O stretching frequency and the average of the σ_p Hammett parameter [45] of *para*-X-aryl substituents (σ_p = −0.17 for Me and 0.53 for CF_3): $\nu_{CO} = 13.984[(\Sigma\sigma_p)/2] + 1954.9$, $R^2 = 0.987$ (see Fig. 4). By comparison of C–O stretching frequencies for **1**–**6** with those of other pincer complexes with various donor sets, it is apparent that the electronic nature of the amido nitrogen anchor *trans*- to the carbonyl rather than the type of flanking Lewis donors in pincer complexes dictates the energy of the C–O stretching vibrations, as might be expected. That is, the ν_{CO} range of 1948–1968 cm^{-1} for **1**–**6** is comparable to the frequency of 1967 cm^{-1} found in cationic carbonylrhodium(I) complexes with bis(carbene)-based pincers of the type 2,6-bis(alkylimidazol-2-ylidene)-pyridine [46] and is between those frequencies found for carbonylrhodium(I) complexes of carbazole-based pincers 1,8-bis(imidazolin-2-yliden-1-yl)carbazolide (CNC-bimca, 1916 cm^{-1}) [18] or 1,8-di(phenylimino)-3,6-dimethylcarbazolides (R = Ph in Chart 1 **F**, 1980 cm^{-1}) [24]. These ν_{CO} values for **1**–**6** are also comparable to 1957 cm^{-1} found for the charge-neutral $Rh(PEt_3)_2(CO)I$ [47], and to 1961 cm^{-1} for $Rh(Cp)(CO)(PPh_3)$ [48].

4.4. Spectroscopic studies of oxidative addition reactions

Given the electron-rich nature of **1**–**6**, oxidative addition reactions with MeI, EtI, and, in one case, I_2 were investigated to determine whether any reaction would occur, and if so, to discern to what extent, if at all, the reaction rates or the nature of the products were affected by the different *para*-X-aryl or 3-R-pyrazolyl substituents. Indeed, IR and NMR spectroscopic studies verified that oxidative addition reactions occurred in all cases, as illustrated in Scheme 3. That is, the original IR band centered in the ν_{CO} range of 1948–1968 $cm^{-1}$of each spectrum of **1**–**6** in acetone was

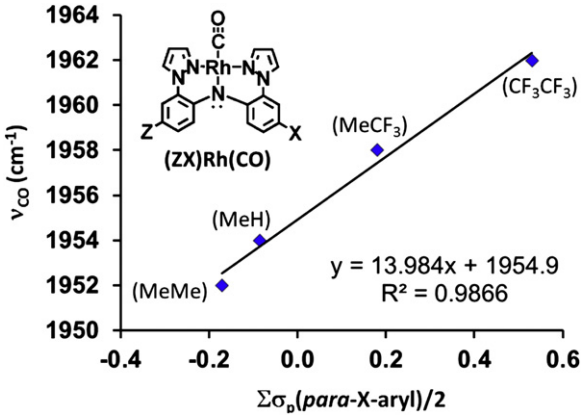

Fig. 4. Correlation between the C–O stretching frequency and the average of the σ_p Hammett parameters (σ_p = 0 for H, −0.17 for Me, and 0.53 for CF_3) of *para*-X-aryl substituents in various (ZX)Rh(CO) pincer complexes.

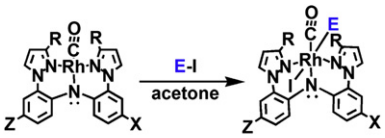

(L)Rh(E)(CO)(I)			$\nu_{C\text{-}O}$ (cm^{-1})
Ligand	E	(#)	(acetone)
MeMe	Me	(7_{Me})	2063
	Et	(7_{Et})	2054
	I	(7_{I})	2078
^{Me}MeMe	Me	(8_{Me})	2057
	Et	(8_{Et})	2052
^{iPr}MeMe	Me	(9_{Me})	2051
	Et	(9_{Et})	2047
MeH	Me	(10_{Me})	2069
	Et	(10_{Et})	2067
$MeCF_3$	Me	(11_{Me})	2069
	Et	(11_{Et})	2067
CF_3CF_3	Me	(12_{Me})	2075
	Et	(12_{Et})	2070

Scheme 3. Summary of oxidative addition reactions of **1**–**6** to form $\mathbf{7_E}$–$\mathbf{12_E}$.

replaced by a new band in the range 2047–2078 cm^{-1} for the appropriate (^{R}ZX)Rh(E = Me or Et)(CO)(I) complexes $\mathbf{7_E}$–$\mathbf{12_E}$, as per Scheme 3. The original set of hydrogen resonances were replaced cleanly with new sets of NMR signals after reaction with alkyl iodides, as exemplified for the formation of $\mathbf{7_{Et}}$ in Fig. 5. It is likely that all complexes share the configuration with alkyl and iodide groups *trans*- to one another, as shown in Scheme 3, given: i) the solid-state structural studies of three derivatives ($\mathbf{7_{Et}}$, $\mathbf{7_I}$, and $\mathbf{8_{Me}}$,vide infra), ii) the similarity in IR and NMR spectroscopic data for all complexes (for instance, a *cis*-configuration is expected to lead to drastically different ν_{CO} stretching frequencies due the *trans*-effect), and iii) because, kinetically, oxidative addition of alkyl halides to square planar d^8 complexes typically lead to *trans*-disposition of added fragments [49]. The different non-pincer (alkyl and iodide) ligands differentiate the "arms" of the non-planar pincer ligand and gives low (C_1) symmetry to the complexes. For a *trans*-disposition of alkyl and iodide ligands as indicated in Scheme 3, one pincer arm is proximal to the iodide group while the second pincer arm is closer to the alkyl group E. Thus, two sets of pyrazolyl and aryl hydrogen resonances are found in the NMR spectrum for the rhodium(III) complexes $\mathbf{7_E}$–$\mathbf{9_E}$ and $\mathbf{12_E}$ (E = Me, Et). The NMR spectra for complexes $\mathbf{10_E}$ and $\mathbf{11_E}$ (E = Me, Et) with different pincer arms (a *p*-tolyl and either a phenyl or a *p*-trifluoromethylaryl, respectively) are more complicated because two isomers are present in each. The isomers can be distinguished by the position of the pincer arms relative to the iodide ligand. One possible isomer places the iodide ligand in van der Waals contact with the tolyl arm of the diarylamido anchor while the second isomer places the halide in contact with the other (phenyl or trifluoromethylaryl) arm, as shown in Fig. 6. Molecular mechanics and semi-empirical (PM3) equilibrium geometry calculations indicate that the isomer with the iodide ligand in van der Waals contact with the less electron-rich *p*-trifluoromethylaryl ring, left of Fig. 6, is lower energy than the isomer with the iodide group in contact with the more electron-rich tolyl group, right of Fig. 6. Integration of well-resolved signals in the 3/5-Hpz and Rh-alkyl regions of the ^{1}H NMR spectrum of $\mathbf{10_E}$ and $\mathbf{11_E}$ (E = Me, Et) indicate a 10:9 relative ratio of isomers for $\mathbf{10_E}$ and a 7:3 ratio for $\mathbf{11_E}$. Thus, empirically, the two isomers (or pathways to them) are nearly equal in energy but the very different electronic properties between CF_3 and CH_3 groups in $\mathbf{11_E}$ versus the H and CH_3 groups in $\mathbf{10_E}$ gives a greater preference for one isomer over the other.

4.5. Kinetic studies of oxidative addition reactions

The reactions between 0.03 M **1**–**6** in acetone-d_6 and 10-fold excess iodomethane were instantaneously complete (at least within seconds) at 295 K. By performing similar reactions at 295 K but in the less polar solvent benzene, the oxidative addition reaction of MeI to **1** was instantaneously complete but those reactions involving complexes with trifluoromethyl-pincer substituents (**5** and **6**) were slow enough to measure pseudo-first order rate constants. In these latter two cases, the pseudo-first order half-life, $t_{1/2}$, was on the order of 1 min for **5** and 26 min for **6**. Qualitatively, the instantaneous reactions in acetone parallel a similar observation reported for (CNC-bimca)Rh(CO) which was found by stopped-flow spectroscopic measurements to exhibit the highest rate for the oxidative addition of CH_3I by a rhodium(I) complex ($k_2 = 3.4 \times 10^{-3}\ M^{-1}\ s^{-1}$, 196 K in THF) [18]. The rapidity of the oxidative addition of **1**–**6** with iodomethane prompted examination of reactions with iodoethane. It is known [48–50] that the rate of oxidation addition of iodoethane to rhodium(I) complexes is generally about 100–1000 times slower than those reactions involving iodomethane because the added steric bulk

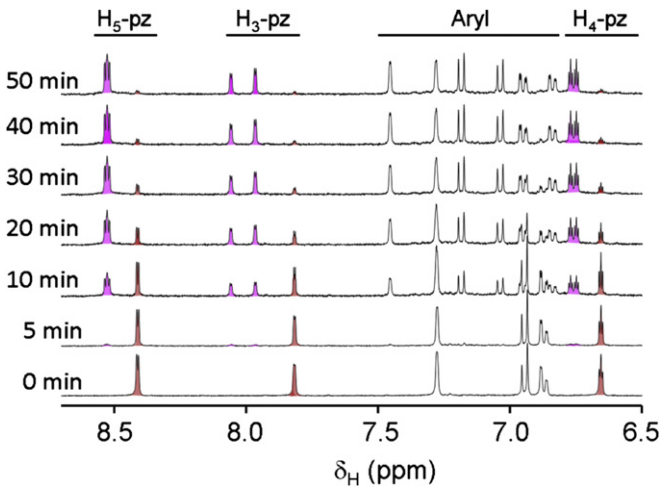

Fig. 5. The downfield region of the ^{1}H NMR spectra during heating a 1:10 mixture of **1**: EtI in acetone-d_6 at 45 °C to form $\mathbf{7_{Et}}$. The resonances for pyrazolyl hydrogens are shaded.

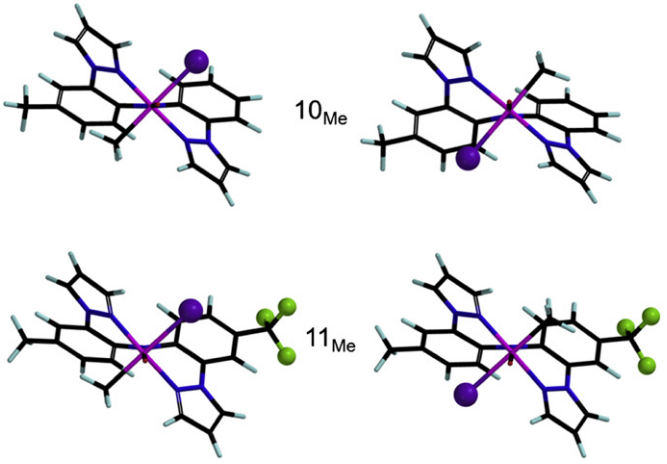

Fig. 6. Two low-energy isomers of $\mathbf{10_{Me}}$ (top) and $\mathbf{11_{Me}}$ (bottom) from PM3 calculations. The isomers on the left with the iodide (purple ball) closer to phenyl or trifluoromethylaryl are slightly lower energy than the isomers on the right. (For interpretation of the references to colour in this figure legend, the reader is referred to the web version of this article.)

Table 5
Summary of kinetic data for reactions between (^{R}ZX)Rh(CO) and iodoethane in acetone-d_6.

(^{R}ZX)Rh(CO) Complex	[Rh], M	[EtI], M	k_2 (318K), M^{-1} s^{-1}	$\Delta^{\ddagger}H^{\circ}$, kJ mol^{-1}	$\Delta^{\ddagger}S^{\circ}$, J K^{-1} mol^{-1}	$\Delta^{\ddagger}G_{318}{}^{\circ}$, kJ mol^{-1}
1	0.031	0.31	8.0×10^{-3}	59	-9.8×10^{1}	90
2	0.030	0.30	1.6×10^{-3}	54	-1.3×10^{2}	95
3	0.025	0.25	1.4×10^{-3}	52	-1.4×10^{2}	97
4	0.034	0.34	7.9×10^{-3}	54	-1.2×10^{2}	91
5	0.025	0.25	2.5×10^{-3}	49	-1.4×10^{2}	94
6	0.026	0.26	8.2×10^{-4}	50	-1.5×10^{2}	98

‡ Standard activation enthalpy, entropy, and free energy as defined/found in the Dec. 2010 IUPAC gold book.

hinders the S_N2-attack by rhodium(I). This strategy permitted successful evaluation of rate constants and activation parameters for reactions involving the entire series of complexes **1**–**6**, as summarized in Table 5. At 318 K, linear plots of *ln* [(^{R}ZX)Rh(CO)] versus time were obtained which showed that the reactions were first order in each **1**–**6**. Moreover, plots of k_{obs} versus [EtI] were linear, indicating the reaction to be first order in EtI and, therefore, second order overall as in Equation (1). The activation parameters for the

$$\text{rate} = k_2[(^{R}\text{ZX})\text{Rh(CO)}][\text{EtI}] \quad (1)$$

reactions between EtI and each carbonylrhodium(I) complex were obtained by Eyring analyses of data from experiments performed at various temperatures between 303 and 323 K, see Supplementary data. As typical for rhodium(I) chemistry, the activation entropies are all large and negative, characteristic of a highly-organized transition state for oxidative addition reactions that proceed by an S_N2 mechanism [50]. Such a mechanism is also suggested from comparison of rate constants of reactions involving **1**–**3**. Complex **1** is the least electron-rich of the three from IR data, yet the reaction with EtI is the fastest. Complex **3** is the most electron-rich owing to the presence of ^{i}Pr pyrazolyl substituents but it reacts slowest of the three complexes owing to steric bulk. Sequential substitution of methyl groups in **1** for hydrogen (in **4**) or electron-withdrawing trifluoromethyl groups (in **5** and **6**) results in predictably slower reactions. There is a good linear correlation between log k_2 and the average of the Hammett parameter, σ_p, for the *p*-X-aryl substituents, log $k_2 = -1.494(\Sigma\sigma_p/2) - 2.3013$ ($R^2 = 0.987$; see ESI for the plot), which signifies that remote electronic effects can provide a powerful means to fine-tune reactivity in these systems without interfering with the steric profile near the metal center.

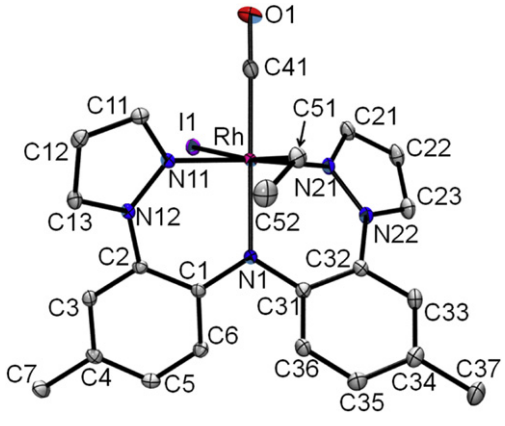

Fig. 7. Structure of (MeMe)Rh(Et)(CO)(I), $\mathbf{7_{Et}}$, with hydrogens removed for clarity. Selected bond distances (Å): Rh1–N1, 2.035(1); Rh1–N11, 2.011(1); Rh1–N21, 2.030(1); Rh1–C51, 2.110(2); Rh1–C41, 1.890(2); C41–O1, 1.126(2); Rh1–I1, 2.8708(2); Selected bond angles (°): N1–Rh1–C41 179.41(7); N11–Rh1–N21 175.25(6); I1–Rh1–C51, 173.17(5); N1–Rh1–N11, 88.96(5); N21–Rh1–N1, 86.62(6); C41–Rh1–I1, 83.67(6); C41–Rh1–C51, 89.50(7).

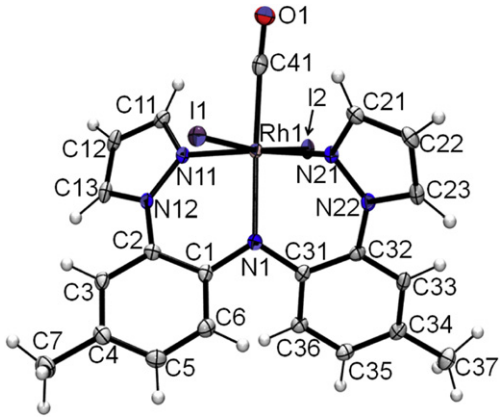

Fig. 8. Structure of (MeMe)Rh(I)$_2$(CO), $\mathbf{7_I}$. Selected bond distances (Å): Rh1–N1, 2.024(2); Rh1–N11, 2.020(2); Rh1–N21, 2.023(2); Rh1–C41, 1.916(3); C41–O1, 1.102(4); Rh1–I1, 2.6907(3); Rh1–I2, 2.6784(3); Selected bond angles (°): N1–Rh1–C41 176.8(1); N11–Rh1–N21 174.4(1); N1–Rh1–N11, 86.8(1); N21–Rh1–N1, 87.7(1); C41–Rh1–I1, 89.0(1); C41–Rh1–I2, 83.9(1); I1–Rh1–I2, 172.83(1).

4.6. Synthetic studies of oxidative addition reactions

During attempts to isolate bulk quantities of $\mathbf{7_E}$–$\mathbf{12_E}$ (E = Me, Et, or I, as appropriate) for further reaction chemistry it was discovered that these complexes were metastable. In fact, we have only been successful at isolating complexes $\mathbf{7_{Me}}$, $\mathbf{7_I}$, and $\mathbf{8_{Me}}$ as analytically pure solids from synthetic-scale (decigram to gram scale) reactions performed in acetone or benzene. All other complexes in Scheme 3 give mixtures from preparative-scale reactions in benzene or acetone owing to various competitive decomposition reactions that appear to be accelerated by excess CH_3I, donor solvents, and by solvent removal, as described later. The ability to isolate $\mathbf{7_{Me}}$, $\mathbf{7_I}$, and $\mathbf{8_{Me}}$ in bulk, pure form is due to the combination of the rapidity of their preparative oxidative addition reactions and the relatively slow rates of their decomposition reactions. Thus, mixing benzene solutions of **1** or **2** and iodomethane or of **1** and iodine for a minimum amount of time required for complete reaction as monitored by IR or NMR spectroscopy, followed by removing volatiles under vacuum gave quantitative yields of the desired

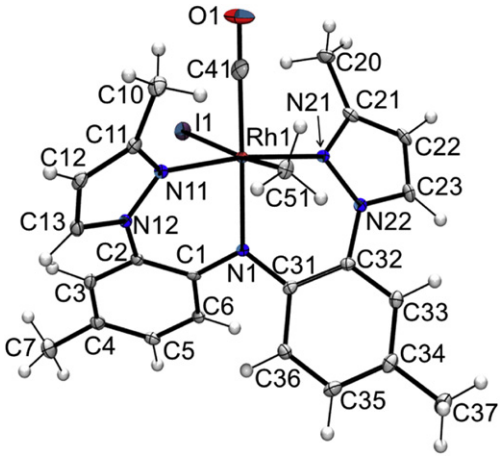

Fig. 9. Structure of (^{Me}MeMe)Rh(Me)(CO)(I) in the crystal of $\mathbf{8_{Me}}\cdot C_6H_6$. Selected bond distances (Å): Rh1–N1, 2.035(2); Rh1–N11, 2.052(3); Rh1–N21, 2.046(3); Rh1–C41, 1.892(3); C41–O1, 1.126(4); Rh1–C51, 2.093(3), Rh1–I1, 2.8604(3); Selected bond angles (°): N1–Rh1–C41 179.7(1); N11–Rh1–N21 172.9(1); N1–Rh1–N11, 86.6(1); N21–Rh1–N1, 86.6(1); C51–Rh1–I1, 175.6(1); C41–Rh1–C51, 90.4(1).

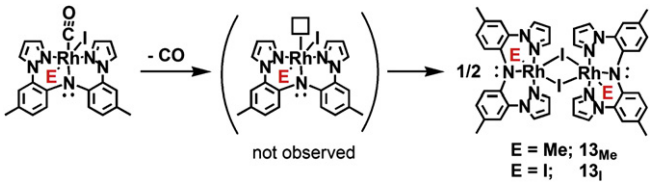

Scheme 4. Unexpected decomposition reactions of $\mathbf{7_E}$ to form dimeric species $\mathbf{13_E}$.

rhodium(III) species as red-orange or orange air-stable powders. Complex $\mathbf{8_{Me}}$ exhibits relatively low solubility in benzene or acetone compared to the other new complexes and precipitates as X-ray quality crystals from unstirred solutions. The other two isolable complexes are soluble in CH_2Cl_2 and acetone, however, solutions begin to deposit insoluble decomposition products (vide infra) over the course of several hours at room temperature. It is possible to isolate a few X-ray quality crystals of various other 'metastable' complexes if the rate of crystallization competes with the rate of decomposition. Thus, a few X-ray quality crystals of $\mathbf{7_{Et}}$ and $\mathbf{7_I}$ were obtained along with copious decomposition products (vide infra) by allowing a layer of hexane to diffuse into a CH_2Cl_2 solution of $\mathbf{7_{Et}}$ or by slow evaporation of an acetone solution of $\mathbf{7_I}$, over the course of a day. The structures of $\mathbf{7_{Et}}$, $\mathbf{7_I}$, and $\mathbf{9_{Me}}$ are found in Figs. 7–9, respectively. Each structure verified the *trans*-disposition of the added iodide and/or alkyl ligands. The biggest difference between common fragments in the structures of **1**, $\mathbf{7_{Et}}$ and $\mathbf{7_I}$ involve the metal-carbonyl moieties. The Rh–C41 bond of 1.890(2) Å in $\mathbf{7_{Et}}$ and of 1.916(3) Å in $\mathbf{7_I}$ is each longer than that of 1.832(2) Å in **1**. The C–O bond distance of 1.126(4) Å in $\mathbf{7_{Et}}$ and 1.102(4) Å in $\mathbf{7_I}$ are also shorter than that of 1.148(3) Å in **1**. These structural differences can be explained by the expected relative capability for a rhodium(III) versus a rhodium(I) center to engage in back-bonding to the carbonyl group. The greater electron σ-donating character of an alkyl versus iodide groups, first evident in IR spectra of $\mathbf{7_{Et}}$ and $\mathbf{7_I}$, is also manifest in the discrepancy in the bond distances of the rhodium-carbonyl fragment in $\mathbf{7_{Et}}$ versus $\mathbf{7_I}$. Surprisingly, the Rh–N bonds and associated angles about the metal–pincer moiety in the three complexes **1**, $\mathbf{7_{Et}}$, and $\mathbf{7_I}$ are remarkably similar with Rh1–N1, 2.035(1), 2.024(2), and 2.036(2) Å for $\mathbf{7_{Et}}$, $\mathbf{7_I}$, and **1**, respectively. Likewise, the average Rh–N_{pz} distances of 2.021(1), 2.022(2), and 2.024(1) Å for $\mathbf{7_{Et}}$, $\mathbf{7_I}$, and **1**, respectively, are essentially equivalent. The bond distances involving the carbonyl moiety in $\mathbf{8_{Me}}$ (Rh1–C41, 1.892(3) Å, C41–O1, 1.126(4) Å) are in accord with a lower degree of metal-carbonyl back-bonding compared to that in **2** (Rh1–C41, 1.813(2) Å, C41–O1, 1.154(3) Å). The Rh1–N1 amido bond distance in $\mathbf{8_{Me}}$ of 2.035(2) Å is statistically-indistinguishable from that in **2** of 2.039(2) Å. In contrast, there is a significant difference in average Rh–N_{pz} bond distances between those in $\mathbf{8_{Me}}$, 2.049(3) Å, and in **2**, 2.036(2) Å. Presumably unfavorable steric interactions between 3-methylpyrazolyl substituents and axial methyl and iodo groups are important enough to cause Rh–N_{pz} bond lengthening in the rhodium(III) complex relative to the rhodium(I) center in **2**.

Complexes $\mathbf{7_E}$, $\mathbf{10_E}$, $\mathbf{11_E}$ and $\mathbf{12_E}$ (with un-substituted pyrazolyl groups on the pincer ligand) decompose over the course of several hours with CO dissociation to give highly insoluble iodide-bridged dimers, exemplified for the conversion of $\mathbf{7_E}$ to crystallographically-verified cases of dimeric $\mathbf{13_E}$ (E = Me, I) in Scheme 4. Views of the structure of $\mathbf{13_I}$ are found in Fig. 10 while that of $\mathbf{13_{Me}}$ is given in the Supplementary data. The rhodium–amido nitrogen bond distance in $\mathbf{13_I}$, Rh1–N1 2.006(5) Å, is significantly shorter than those found in **1**, 2.036(2) Å, $\mathbf{7_{Et}}$, 2.035(1) Å, or $\mathbf{7_I}$, 2.024(2) Å.

Again, the average Rh–N_{pz} 2.026(5) Å in $\mathbf{13_I}$ is invariant across this series of complexes. Also, the terminal Rh1–I2 bond distance of 2.6478(6) Å in $\mathbf{13_I}$ is slightly shorter than the range of Rh–I distances found among the two crystallographically-independent units in $\mathbf{7_I}$ of 2.6768(3) to 2.6984(3) Å. The centrosymmetric Rh_2I_2 metallacycle of $\mathbf{13_I}$ has two shorter 2.6812(6) Å Rh–I bonds and two longer 2.7215(6) Å Rh–I bonds similar to other complexes with an Rh_2I_2 core [51]. The non-bonded Rh···Rh and I···I distances within the metallacycle of $\mathbf{13_I}$ are 4.0222(7) and 3.6071(6) Å, respectively. The longer Rh–I bonds of the metallacycle in $\mathbf{13_I}$ are *trans*- to the terminal Rh1–I2 or Rh1′–I2′ bonds. A similar geometry with longer Rh–I bonds of the metallacycle being situated *trans*- to terminal ligands persists in the structure of $\mathbf{13_{Me}}$. It is noted that the structure of $\mathbf{13_{Me}}$ displays about a 9% substitution of methyls for iodides or could be considered a 91:9 co-crystal of $\mathbf{13_{Me}}$:$\mathbf{13_I}$. Thus, the decomposition pathway is likely more complicated than simple CO dissociation and subsequent oligomerization, as depicted in Scheme 4.

4.7. Electrospray mass spectrometry studies of decomposition products

The electrospray ionization mass spectra, ESI (+) MS, for various complexes ($7_{\mathbf{E=Me,\ Et,\ I}}$, $\mathbf{8_{E=Me,\ Et}}$, $\mathbf{13_{E=Me,\ I}}$) were acquired for added characterization and as an attempt to provide further insight into the nature of the solution decomposition of $\mathbf{7_E}$ and $\mathbf{8_E}$. The results of these studies suggest that insoluble dimeric species are the ultimate decomposition products of pincer complexes $7_{\mathbf{E=Me,Et}}$ with un-substituted pyrazolyl donors whereas soluble, monomeric species are the likely the ultimate decomposition products of pincer complexes $\mathbf{8_{E=Me,Et}}$ with 3-methylpyrazolyl donors. The spectrum of $\mathbf{7_I}$ as a CH_3CN solution showed only three main signals at $m/z = 713$ for $[(MeMe)RhI_2(CO)]^{\bullet+}$, $m/z = 714$ (100% relative intensity) for

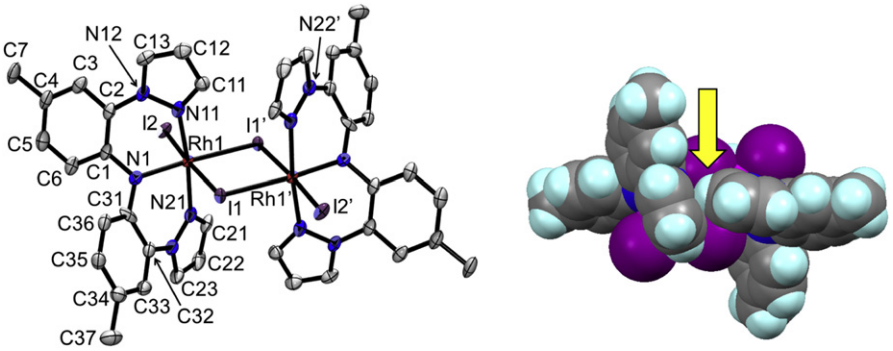

Fig. 10. Left: Structure of $[(MeMe)Rh(I)(\mu\text{-}I)]_2$, $\mathbf{13_I}$, with atom labeling and hydrogens removed for clarity. Selected bond distances (Å): Rh1–N1, 2.006(5); Rh1–N11, 2.018(5); Rh1–N21, 2.034(5); Rh1–I1′, 2.6812(6); Rh1–I1, 2.7215(6); Rh1–I2, 2.6478(6); Selected bond angles (°): N1–Rh1–I1′ 176.2(2); N11–Rh1–N21, 173.5(2); N11–Rh1–N1, 87.1(2); N21–Rh1–N1, 86.8(2); I1–Rh1–I2, 174.03(2); I1–Rh1–I1′, 83.77(2); I2–Rh1–I1′, 90.3(2); Right: Space-filling structural representation with arrow denoting potential steric interactions between pyrazolyl rings.

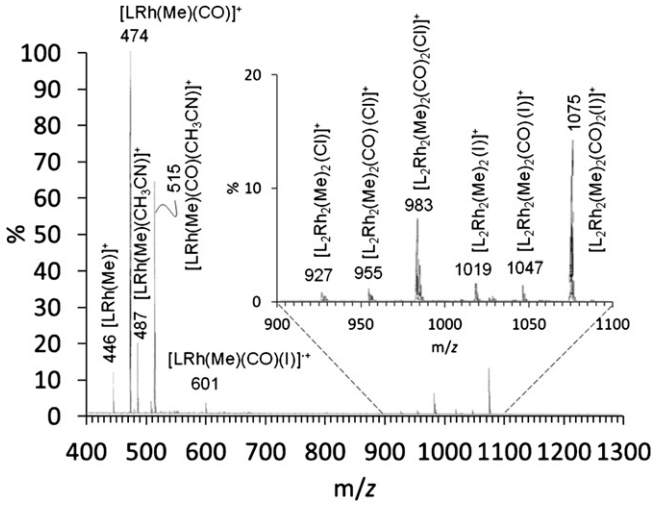

Fig. 11. ESI(+) mass spectrum for a CH_3CN solution of (MeMe)Rh(Me)(CO)(I), $\mathbf{7_{Me}}$.(the chloride comes from the common anion impurity in the ESI(+) experiment rather than from the sample).

$[H(MeMe)RhI_2(CO)]^+$, and at $m/z = 726$ for $[(MeMe)RhI(CH_3CN)]^+$. All the other complexes showed more complex fragmentation patterns with peaks in the region between ca. $m/z = 450$ to 750 for monomeric cations and between ca. $m/z = 925$ to 1400 for dimeric cations, as exemplified for $\mathbf{7_{Me}}$ in Fig. 11. The data for the other complexes can be found in the Supplementary data. The 100% relative intensity signal for complexes other than $\mathbf{7_I}$ were for monomeric cations- either $[LRh(alkyl)(CO)]^+$, $[LRh(alkyl)(CH_3CN)_{x=1,2}]^+$, or $[LRh(alkyl)(CO)(CH_3CN)]^+$ depending on the complex or experimental run (some spectra were acquired multiple times using different samples of a given complex). Thus, dissociation of one iodide is a predominant fragmentation pattern in each complex, CO loss is also common for all, and rhodium-alkyl fragmentation is more prevalent in $\mathbf{8_{E=Me,Et}}$ than in $\mathbf{7_{E=Me,Et}}$. The data also suggest that the new pincer ligands are capable of supporting coordinatively-unsaturated rhodium(III) species such as $[LRh(alkyl)]^+$, at least under these experimental conditions. The observation of peaks in the m/z range above 950 in the mass spectra of $\mathbf{8_{E=Me,Et}}$ demonstrate that dimeric cations can still form after/with loss of an initial iodide or carbonyl ligand despite the added steric bulk on the pyrazolyls in $\mathbf{8_{E=Me,Et}}$. This result was initially surprising since inspection of the structure of the related $\mathbf{13_E}$ suggested that unfavorable steric interactions between 3-organopyrazolyl groups (as indicated by the yellow arrow in the right of Fig. 10, for instance) might preclude association. When CD_2Cl_2 solutions of $\mathbf{8_E}$ were allowed to decompose over the period of two weeks, peaks for dimeric species derived from fragmentation of $\mathbf{8_E}$ (and $\mathbf{9_E}$) were no longer present in the ESI(+) spectrum. Instead, peaks for new monomeric ions were observed that were clearly different than those expected based on the ESI(+) mass spectra of the insoluble decomposition products of $\mathbf{7_E}$, formed under similar conditions. Unfortunately, the identity of the ultimate product(s) of decomposition of $\mathbf{8_E}$ remains uncertain despite multiple attempts at monitoring the decomposition reaction by both ^1H NMR spectroscopic and ESI(+) mass spectral studies (see Supplementary data for more details).

5. Concluding remarks

A convergent method to prepare pyrazolyl-containing pincer ligands is reported that uses CuI as an inexpensive amination catalyst rather than the more typical palladium or bulky phosphine catalyst systems.This synthetic methodology affords ready access to pincer scaffolds with different aryl 'arms' and permits systematic investigations of the roles that electronics and sterics can have on their coordination chemistry. For rhodium chemistry described here, we have demonstrated that it was possible to isolate carbonylrhodium(I) complexes using two different synthetic routes. The rates of oxidative addition reactions involving these new carbonylrhodium(I) pincer complexes varied in a regular manner with different steric requirements of 3-pyrazolyl substituents or the electronic donating character of the *para*-X-aryl pincer substituents. Thus, replacing *para*-methyl groups of the tolyl pincer 'arms' with trifluoromethyls gave less electron-rich rhodium(I) centers, as gauged by increasing ν_{CO} IR stretching frequencies, and ultimately slowed the rates of oxidative addition reactions with alkyl iodides. The replacement of hydrogen at the 3-position of the pyrazolyls (closest to the metal center) with methyl or isopropyl groups resulted in more electron-rich rhodium(I) centers along series MeMe < MeMeMe < ^{iPr}MeMe due to inductive effects. However, oxidative addition reactions with alkyl iodides became progressively slower with increasing steric bulk of 3-pyrazolyl substituents. The resultant rhodium(III) complexes were found to be unstable and decomposed with loss of CO regardless of substitution pattern on the pincer ligand. The one difference in the decomposition products is that those with unsubstituted pyrazolyls were insoluble dimeric species that were doubly iodide-bridged while those with 3-organopyrazolyl derivatives were soluble and likely monomeric in nature from ESI(+) mass spectral studies. The different stabilities of the rhodium(III) complexes of the new NNN-pincers reported here and those of related NNN- or NCN pincer ligands underscores the importance of ligand donor atoms and of chelate ring size on the reactivities of metal pincer complexes. Given the synthetic advances reported here and those reported elsewhere for accessing new pyrazole variants [52], the full potential of the new pincer ligands and their metal complexes in stoichiometric and catalytic reactions are currently being investigated in our laboratory and results will be reported in due course.

Acknowledgments

JRG thanks Marquette University and the National Science Foundation (CHE-0848515) for financial support.

Appendix A. Supplementary material

CCDC 87623–87632 contain the supplementary crystallographic data for **1**–**3**, $\mathbf{4}\cdot C_6H_6$, **5**, $\mathbf{7_{Et}}$, $\mathbf{7_I}\cdot$1.5acetone, $\mathbf{8_{Me}}\cdot C_6H_6$, $\mathbf{13_{Me}}\cdot$acetone, and $\mathbf{13_I}\cdot Et_2O$. These data can be obtained free of charge from The Cambridge Crystallographic Data Centre via www.ccdc.cam.ac.uk/data_request/cif.

Appendix. Supplementary data

Supplementary data associated with this article can be found, in the online version, at doi:10.1016/j.jorganchem.2011.08.013.

References

[1] C.J. Moulton, B.L. Shaw, J. Chem. Soc. Dalton Trans. (1976) 1020–1024.
[2] D. Morales-Morales, C. Jensen (Eds.), The Chemistry of Pincer Compounds, Elsevier, Amsterdam, 2007.
[3] (a) G. van Koten, J.T.B.H. Jastrzebski, J.G. Noltes, A.L. Spek, J.C. Schoone, J. Organomet. Chem. 148 (1978) 233–245;
(b) G. van Koten, K. Timmer, J.G. Noltes, A.L. Spek, J. Chem. Soc. Chem. Commun. (1978) 250–252;
(c) G. van Koten, Pure Appl. Chem. 61 (1989) 1681–1694.
[4] (a) A.A.H. van der Zeijden, G. van Koten, R. Luijk, K. Vrieze, C. Slob, H. Krabbendam, A.L. Spek, Inorg. Chem. 27 (1988) 1014–1019;

(b) A.A.H. van der Zeijden, G. van Koten, R.A. Nordemann, B. Kojić-Rodić, A.L. Spek, Organometallics 7 (1988) 1957–1966;
(c) A.A.H. van der Zeijden, G. van Koten, J.M. Ernsting, C.J. Elsevier, B. Krijnen, C.H. Stam, J. Chem. Soc. Dalton Trans. (1989) 317–324.
[5] (a) M. Albrecht, M.M. Lindner, Dalton Trans. 40 (2011) Advanced Article, doi:10.1039/c1dt10339c;
(b) J. Choi, A.H.R. MacArthur, M. Brookhart, A.S. Goldman, Chem. Rev. 111 (2011) 1761–1779;
(c) N. Selander, K.J. Szabó, Chem. Rev. 111 (2011) 2048–2076.
[6] (a) L.-C. Liang, J.-M. Lin, C.-H. Hung, Organometallics 22 (2003) 3007–3009;
(b) See also asymmetric derivatives: R.B. Lansing Jr., K.I. Goldberg, R.A. Kemp Dalton Trans. 40 (2011) Advanced Article, doi:10.1039/c1dt10265f.
[7] (a) P. Surawatanawong, O.V. Ozerov, Organometallics 30 (2011) 2972–2980;
(b) M. Puri, S. Gatard, D.A. Smith, O.V. Ozerov, Organometallics 30 (2011) 2472–2485;
(c) S. Gatard, C.-H. Chen, B.M. Foxman, O.V. Ozerov, Organometallics 27 (2008) 6257–6267;
(d) S. Gatard, C. Guo, B.M. Foxman, O.V. Ozerov, Organometallics 26 (2007) 6066–6075;
(e) S. Gatard, R. Çelenligil-Çetin, C. Guo, B.M. Foxman, O.V. Ozerov, J. Am. Chem. Soc. 128 (2006) 2808–2809.
[8] A.M. Winter, K. Eichele, H.-G. Mack, S. Potuznik, H.A. Mayer, W.C. Kaska, J. Organomet. Chem. 682 (2003) 149–154.
[9] M. Feller, M.A. Iron, L.J.W. Shimon, Y. Diskin-Posner, G. Leitus, D. Milstein, J. Am. Chem. Soc. 130 (2008) 14374–14375.
[10] (a) A.Y. Verat, H. Fan, M. Pink, Y.-S. Chen, K.G. Caulton, Chem. Eur. J. 14 (2008) 7680–7686;
(b) A.Y. Verat, M. Pink, H. Fan, J. Tomaszewski, K.G. Caulton, Organometallics 27 (2008) 166–168.
[11] (a) W.-W. Xu, G.P. Rosini, M. Gupta, C.M. Jensen, W.C. Kaska, K. Krogh-Jespersen, A.S. Goldman, Chem. Commun. (1997) 2273–2274;
(b) M. Gupta, C. Hagen, R.J. Flesher, W.C. Kaska, C.M. Jensen, Chem. Commun. (1996) 2083–2084 and 2687.
[12] (a) M. Montag, I. Efremenko, R. Cohen, L.J.W. Shimon, G. Leitus, Diskin-Y. Posner, Y. Ben-David, H. Salem, J.M.L. Martin, D. Milstein, Chem. Eur. J. 16 (2010) 328 (and references);
(b) C.M. Frech, D. Milstein, J. Am. Chem. Soc. 128 (2006) 12434–12435.
[13] D.F. MacLean, R. McDonald, M.J. Ferguson, A.J. Caddell, L. Turculet, Chem. Commun. (2008) 5146–5148.
[14] M. Delferro, M. Tegoni, V. Verdolino, D. Cauzzi, C. Graiff, A. Tiripicchio, Organometallics 28 (2009) 2062–2071.
[15] M. Doux, L. Ricard, P. Le Foch, Y. Jean, Organometallics 25 (2006) 1101–1111.
[16] M.E. El-Zaria, H. Arii, H. Nakamura, Inorg. Chem. 50 (2011) 4149–4161.
[17] (a) T. Zweifel, J.-V. Naubron, H. Grützmacher, Angew. Chem. Int. Ed. 48 (2009) 559–563;
(b) T. Büttner, J. Geier, G. Frison, J. Harmer, C. Calle, A. Schweiger, H. Schönberg, H. Grützmacher, Science 307 (2005) 235–238.
[18] (a) B. Wucher, M. Moser, S.A. Schumacher, F. Rominger, D. Kunz, Angew. Chem. Int. Ed. 48 (2009) 4417–4421;
(b) M. Moser, B. Wucher, D. Kunz, F. Rominger, Organometallics 26 (2007) 1024–1030.
[19] Ligand A, Chart 1, $n = 1$: (a) S. Radi, S. Tighadouini, Y. Toubi, M. Bacquet, J. Hazard. Mater. 185 (2011) 494–503;
(b) H. Yang, Y. Tang, Z.-F. Shang, X.-L. Han, Z.-H. Zhang, Polyhedron 28 (2009) 3491–3498;
(c) W.L. Driessen, W.G.R. Wiesmeijer, M. Schipper-Zablotskaja, R.A.G. De Graaff, J. Reedijk, Inorg. Chim. Acta 162 (1989) 233–238;
(d) W.L. Driessen, R.A.G. De Graaff, J. Ochocki, J. Reedijk, Inorg. Chim. Acta 150 (1988) 41–45 Ligand A, Chart 1, $n = 2$;
(e) T.N. Sorrell, M.R. Malachowski, Inorg. Chem. 21 (1983) 1883–1887;
(f) S. Alves, A. Paulo, J.D.G. Correia, Â Domingos, I. Santos, J. Chem. Soc. Dalton Trans. (2002) 4714–4719;
(g) S. Alves, A. Paulo, J.D.G. Correia, L. Gano, C.J. Smith, T.J. Hoffman, I. Santos, Bioconjug. Chem. 16 (2005) 438–449.
[20] Ligand B, Chart 1: (a) W.I. Dzik, L.F. Arruga, M.A. Siegler, A.L. Spek, J.N.H. Reek, B. de Bruin, Organometallics 30 (2011) 1902–1913;
(b) W.I. Dzik, C. Creusen, R. de Gelder, T.P.J. Peters, J.M.M. Smits, B. de Bruin, Organometallics 29 (2010) 1629–1641;
(c) C. Tejel, M.P. del Río, M.A. Ciriano, E.J. Reijerse, F. Hartl, S. Záliš, D.G.H. Hetterscheid, N.T.I. Spithas, B. de Bruin, Chem. Eur. J. 15 (2009) 11878–11889;
(d) C. Tejel, M.P. del Río, M.A. Ciriano, M.P. del Río, F.J. van den Bruele, D.G.H. Hetterscheid, N.T.I. Spithas, B. de Bruin, J. Am. Chem. Soc. 130 (2008) 5844–5845;
(e) D.G.H. Hetterscheid, M. Klop, R.J.N.A.M. Kicken, J.M.M. Smits, E.J. Reijerse, B. de Bruin, Chem. Eur. J. 13 (2007) 3386–3405.
[21] Ligand C, Chart 1: F. Konrad, J.L. Fillol, H. Wadepohl, L.H. Gade Inorg. Chem. 48 (2009) 8523–8532.
[22] Ligand D, Chart 1: (a) J.L. Cryder, A.J. Killgore, C. Moore, J.A. Golen, A.L. Rheingold, C.J.A. Daley, Dalton Trans. 39 (2010) 10671–10677;
(b) B.K. Langlotz, H. Wadepohl, L.H. Gade, Angew. Chem. Int. Ed. 47 (2008) 4670–4674.
[23] Ligand E, Chart 1: (a) M. Inoue, M. Nakada, Heterocycles 72 (2007) 133–138;
(b) M. Inoue, M. Nakada, Angew. Chem. Int. Ed. 45 (2006) 252–255.
[24] Ligand F, Chart 1: (a) J.A. Gaunt, V.C. Gibson, A. Haynes, S.K. Spitzmesser, A.J.P. White, D.J. Williams, Organometallics 23 (2004) 1015–1023;
(b) For an alternative ligand preparation, see: A.M. Hollas, W. Gu, N. Bhuvanesh, O.V. Ozerov Inorg. Chem. 50 (2011) 3673–3679.
[25] Ligand G, Chart 1: M.S. Mudadu, A.N. Singh, R.P. Thummel J. Org. Chem. 73 (2008) 6513–6520.
[26] Ligand H, Chart 1: (a) T. Inagaki, A. Ito, J.-I. Ito, H. Nishiyama, Angew. Chem. Int. Ed. 49 (2010) 9384–9387;
(b) H. ;Liu, D.-M. Du, Eur. J. Org. Chem. (2010) 2121–2131.
[27] Ligand I, Chart 1: (a) D.S.C. Black, N.E. Rothnie, Tetrahedron Lett. 31 (1978) 28352838;
(b) D.S.C. Black, N.E. Rothnie, Aust. J. Chem. 36 (1983) 2395–2406;
(c) S.A. Cameron, S. Brooker, Inorg. Chem. 50 (2011) 3697–3699.
[28] Ligand J, Chart 1: (a) P. Ren, O. Vechorkin, Z. Csok, I. Salihu, R. Scopelliti, X. Hu, Dalton Trans. 40 (2011) Advance Article, doi:10.1039/c1dt10195a;
(b) J. Breitenfeld, O. Vechorkin, C. Corminboeuf, R. Scopelliti, X. Hu, Organometallics 29 (2010) 3686–3689;
(c) Z. Csok, O. Vechorkin, S.B. Harkins, R. Scopelliti, X. Hu, J. Am. Chem. Soc. 130 (2008) 8156–8157.
[29] Ligands K and L, Chart 1: (a) J.C. Peters, S.B. Harkins, S.D. Brown, M.W. Day, Inorg. Chem. 40 (2001) 5083–5091;
(b) T.A. Betley, B.A. Qian, J.C. Peters, Inorg. Chem. 47 (2008) 11570–11582.
[30] Other rhodium complexes of NNN-pincers: (a) J.H.H. Ho, D. St Clair Black, B.A. Messerle, J.K. Clegg, P. Turner, Organometallics 25 (2006) 5800–5810;
(b) M. Kooistra, D.G.H. Hetterscheid, E. Schwartz, Q. Knijnenburg, P.H.M. Budzelaar, A.W. Gal, Inorg. Chim. Acta 357 (2004) 2945–2952.
[31] (a) S. Wanniarachchi, B.J. Liddle, J. Toussaint, S.V. Lindeman, B. Bennett, J.R. Gardinier, Dalton Trans. 40 (2011) 8776–8787;
(b) S. Wanniarachchi, B.J. Liddle, J. Toussaint, S.V. Lindeman, B. Bennett, J.R. Gardinier, Dalton Trans. 39 (2010) 3167–3169.
[32] M. Montag, L. Schwartsburd, R. Cohen, G. Leitus, Y. Ben-David, J.M.L. Martin, D. Milstein, Angew. Chem. Int. Ed. 46 (2007) 1901–1903.
[33] M.A.F. Hernandez-Gruel, J.J. Pérez-Torrente, M.A. Ciriano, L.A. Oro, Inorg. Synth. 34 (2004) 128.
[34] (a) B.J. Liddle, R.M. Silva, T.J. Morin, F.P. Macedo, R. Shukla, S.V. Lindeman, J.R. Gardinier, J. Org. Chem. 72 (2007) 5637–5646;
(b) T.J. Morin, S.V. Lindeman, J.R. Gardinier, Eur. J. Inorg. Chem. (2009) 104–110.
[35] SMART APEX2 Version 2.1-4, SAINT+Version 7.23a and SADABS Version 2004/1. Bruker Analytical X-ray Systems, Inc., Madison, Wisconsin, USA, 2005.
[36] CrysAlisPro, Agilent Technologies, Version 1.171.34.46 (release 25-11-2010 CrysAlis171.NET), (compiled Nov 25 2010,17:55:46).
[37] G.M. Sheldrick, SHELXTL Version 6.12. Bruker Anal. X-ray Systems, Inc., Madison Wisconsin, USA, 2001.
[38] SCALE3 ABSPACK – An Oxford Diffraction Program (1.0.4, gui:1.0.3) (C). Oxford Diffraction Ltd, 2005.
[39] (a) H.-J. Cristau, P.P. Cellier, J.-F. Spindler, M. Taillefer, Eur. J. Org. Chem. (2004) 695–709;
(b) M. Taillefer, N. Xia, A. Ouali, Angew. Chem. Int. Ed. 46 (2007) 934–936;
(c) H.-J. Christau, P.P. Cellier, J.-F. Spindler, M. Taillefer, Chem. Eur. J. 10 (2004) 5607–5622;
(d) See also, J.M. Lindley, I.M. McRobbie, O. Meth-Cohn, H. Suschitzky, J. Chem. Soc. Perkin Trans. 1 (1980) 982–994;
(e) J.C. Antilla, J.M. Baskin, T.E. Barder, S.L. Buchwald, J. Org. Chem. 69 (2004) 5578–5587.
[40] B.J. Liddle, J.R. Gardinier, J. Org. Chem. 72 (2007) 9794–9797.
[41] R. Mathieu, G. Esquius, N. Lugan, J. Pons, J. Ros, Eur. J. Inorg. Chem. (2001) 2683–2688.
[42] A. Boixassa, J. Pons, J. Ros, R. Mathieu, N. Lugan, J. Organomet. Chem. 682 (2003) 233–239.
[43] J. García-Anton, R. Mathieu, N. Lugan, J.P. Picart, J. Ros, J. Organomet. Chem. 689 (2004) 1599–1602.
[44] J. Huang, C.M. Haar, S.P. Nolan, W.J. Marshall, K.G. Moloy, J. Am. Chem. Soc. 120 (1998) 7806–7815.
[45] C. Hansch, A. Leo, Substituent Constants for Correlation Analysis in Chemistry and Biology. Wiley-Interscience, New York, 1979.
[46] J.M. Wilson, G.J. Sunley, H. Adams, A. Haynes, J. Organomet. Chem. 690 (2005) 6089–6095.
[47] J. Rankin, A.C. Benyei, A.D. Poole, D.J. Cole-Hamilton, J. Chem. Soc. Dalton Trans. (1999) 3771–3782.
[48] A.J. Hart-Davis, W.A.G. Graham, Inorg. Chem. 9 (1970) 2658–2663.
[49] (a) J.P. Collmann, L.S. Hegedus, J.R. Norton, R.G. Finke, Principles and Applications of Organotransition Metal Chemisty, second ed. University Science Books, Mill Valley, CA, 1987;
(b) R.H. Crabtree, The Organometallic Chemistry of the Transition Metals, fifth ed. Wiley-Interscience, New York, 2009, (Chapter 6 and 12);
(c) P.W.N.M. van Leeuwen, Homogeneous Catalysis: Understanding the Art. Kluwer Academic Publishers, Dordrecht, 2004, (Chapter 2 and 6);
(d) J. Hartwig, Organotransition Metal Chemsitry: From Bonding to Catalysis. University Science Books, Mill Valley, CA, 2010, (Chapters 5–7).
[50] P.R. Ellis, J.M. Pearson, A. Haynes, H. Adams, N.A. Bailey, P.M. Maitlis, Organometallics 13 (1994) 3215–3226 (and references).
[51] (a) R.J. Rubio, G.T.S. Andavan, E.B. Bauer, T.K. Hollis, J. Cho, F.S. Than, B. Donnadieu, J. Organomet. Chem. 690 (2005) 5353–5364;
(b) A. Haynes, P.M. Maitlis, I.A. Stanbridge, S. Haak, J.M. Pearson, H. Adams, N.A. Bailey, Inorg. Chim. Acta 357 (2004) 3027–3037.
[52] S. Fustero, M. Sánchez-Roselló, P. Barrio, A. Simón-Fuentes, Chem. Rev. 111 (2011) ASAP, dx.doi:org/10.1021/cr2000459.